





Two-Timescale Joint Precoding Design and RIS Optimization for User Tracking in Near-Field MIMO Systems

Silvia Palmucci , *Student Member, IEEE*, Anna Guerra , *Member, IEEE*,
Andrea Abrardo , *Senior Member, IEEE*, and Davide Dardari , *Senior Member, IEEE*

Abstract—In this paper, we propose a novel framework that aims to jointly design the reflection coefficients of multiple reconfigurable intelligent surfaces and the precoding strategy of a single base station (BS) to optimize the self-tracking of the position and the velocity of a single multi-antenna user equipment (UE) that moves either in the far- or near-field region. Differently from the literature, and to keep the overall complexity affordable, we assume that RIS optimization is performed less frequently than localization and precoding adaptation. The proposed procedure leads to minimize the inverse of the received power in the UE position uncertainty area between two subsequent optimization steps. The optimal RIS and precoder strategy is compared with the classic beam focusing strategy and with a scheme that maximizes the communication rate. It is shown that if the RISs are optimized for communications, their configuration is suboptimal when used for tracking purposes. Numerical results show that in typical indoor environments with only one BS and a few RISs operating on millimeter waves, high location accuracy in the range of less than half a meter can be achieved.

Index Terms—Reconfigurable intelligent surfaces, Bayesian tracking, MIMO, optimization.

I. INTRODUCTION

LOCATION awareness is an essential feature of sixth-generation cellular communication systems as high-accuracy positioning facilitates low latency and reliable wireless communications, also in indoor or GNSS-deprived environments [1]. Indeed, in harsh electromagnetic (EM) environments achieving high positioning accuracy is a challenging task due to the presence of multipath, cluttering, and non-line-of-sight (NLOS) propagation [2]. Traditional

Manuscript received 2 December 2022; revised 20 April 2023 and 23 June 2023; accepted 14 July 2023. Date of publication 3 August 2023; date of current version 9 September 2023. This work was supported in part by Theory Lab, Central Research Institute, 2012 Labs, Huawei Technologies Co., Ltd., and in part by the European Union under the Italian National Recovery and Resilience Plan (NRRP) of NextGenerationEU, partnership on “Telecommunications of the Future” under Grant PE00000001—program “RESTART.” The associate editor coordinating the review of this manuscript and approving it for publication was Dr. Mingyi Hong. (*Corresponding author: Davide Dardari.*)

Silvia Palmucci and Andrea Abrardo are with the University of Siena, 53100 Siena, Italy (e-mail: silvia.palmucci@student.unisi.it; abrardo@diism.unisi.it).

Anna Guerra is with the National Research Council of Italy, IEIIT-CNR, 40136 Bologna, Italy (e-mail: anna.guerra@cnr.it).

Davide Dardari is with the WiLAB - Department of Electrical and Information Engineering “Guglielmo Marconi” - CNIT, University of Bologna, 40136 Bologna, Italy (e-mail: davide.dardari@unibo.it).

Digital Object Identifier 10.1109/TSP.2023.3300633

solutions to address this issue include the deployment of numerous BSs and the use of advanced signal processing techniques [3] while lower complexity alternatives include passive relays typically made of a single non reconfigurable antenna. More recently, the introduction of intelligent surfaces (ISs), either in active or reflective mode, has been welcomed as a game-changer low-power technology to realize smart radio environments [4]. Thanks to their capability to control the amplitude and phase of the impinging wavefront, RISs can be used to enhance communication performance by focusing the power on interested UEs and by enabling higher data rates [5], [6], [7], [8], [9]. At the same time, thanks to the possibility of constructing such surfaces with large physical apertures that enable an increased angular resolution, they also improve the accuracy of localization systems [10], [11], [12], [13], [14], [15], [16].

The potential benefits of integrating RISs into localization systems have been investigated in several papers. For example, in [17], a single-input single-output (SISO) Orthogonal Frequency Division Multiplexing (OFDM) downlink scenario with a RIS in a far-field regime is analyzed from communication and localization perspective. Similarly, the authors in [10] derive Cramér-Rao lower bound (CRLB) on positioning accuracy in a downlink scenario, highlighting the benefits of employing RISs in far-field over methods that merely utilize the environment’s natural scattering. Instead, the authors in [11] explore the localization performance limits for an uplink multiple-input multiple-output (MIMO) system operating using near-field propagation models, valid for limited distances, demonstrating the improvement in localization accuracy when a single RIS is present. In [14], the impact of an EM lens on near-field positioning performance is investigated through a maximum likelihood estimation analysis, whereas, in [13], the problem of single-anchor localization assisted by RIS is considered for applications characterized by frequent NLOS conditions. Additional practical RIS-aided localization algorithms can be found in [12], [18], [19].

The localization and communication performance severely relies on the design and control of RISs. In this regard, a rich literature is available for optimizing RIS-aided communications under different channel state information (CSI) and/or prior localization knowledge [20], [21], [22]. However it should be

noted that RIS optimization schemes designed to improve communications are not necessarily optimal or effective to increase localization accuracy because the respective performance indicators (e.g., the achievable rate vs. position error bound) depend differently on RIS configuration, channel characteristics, and geometry. Fewer results on RIS optimization dedicated to localization are available. In particular, [23] develops a method for the computation of the UE position through multiple RISs that are alternatively enabled and tuned using a localization-based cost function. The overall problem is expressed as an iterative procedure during which a minimum distance criterion is used to activate a specific RIS and to estimate the UE position. In [24], the authors present a RIS design method based on optimizing a closed-form position error bound (PEB) in the presence of NLOS and considering practical hardware constraints. In [25], a worst-case localization design is proposed based on the minimization of the squared PEB. In [26], an optimization problem for RIS localization and transmit power minimization is presented both for the case of single and multiple targets, using the CRLB and the semidefinite relaxation method for the power optimization problem.

Recently, the localization and communication tasks have been addressed jointly. Along this direction, the paper [27] considers the localization statistics, determined using the Fisher Information Matrix (FIM) of the observation model, and proposes a new framework for integrated localization and communication. Therefore, the subsequent RIS configurations are fixed along a location coherence interval, while the BS precoders are optimized at each channel coherence interval. In [28], a joint communication and localization approach is presented, in which the RIS is designed to maximize the average rate by taking advantage of a RIS-aided tracking procedure. The problem of jointly designing localization and communication is also tackled in [29], where a hierarchical codebook for the RIS phase profile is proposed to enable adaptive bisection search over the angular space.

Most of the existing works entailing RIS-aided localization consider snapshot positioning in the far-field region [2], [11], [12], [13], [23], [26], [29]. In contrast, only a few works consider the UE tracking problem. Among them, in [30], a multiple-antenna BS estimates the position of a multiple-antenna UE and tracks its trajectory through a message-passing algorithm that infers the UE position starting from the estimated angle-of-arrivals. Such an observation model is applicable when the system operates in the far-field and only bearing information can be retrieved to infer the UE position. Moreover, two-step positioning approaches starting from intermediate parameters, e.g., AOA, are suboptimal with respect to direct algorithms and require a proper characterization of the measurement statistics. In the algorithm proposed in [30], both the BS and the RIS design are optimized to minimize the Bayesian CRLB. However, the RIS optimization, designed to focus the reflected power towards the position estimate, does not consider the UE uncertainty area. Moreover, the authors assume that, at each time step and whenever a new position estimate is available, the transmission parameters are optimized, leading to higher system latency and signaling overheads. In general, better

localization performance can be achieved by directional beamforming on the BS side, provided that it is equipped with many antennas and, for the optimal result, that there exists a prior UE location information [31]. Hence, to increase the system degrees of freedom in a RIS-aided environment, the optimization process may involve the joint design of BS precoder and RIS profiles, as it happens in [30]. However, considering that most applications require a high localization update during the tracking process (e.g., 10-100 Hz refresh rate), it is obvious that the optimization of the RIS at the same rates of location update and precoder optimization could be demanding. From the literature, it is well known that performing frequent RIS optimization through channel estimation would pose severe issues in terms of signaling overhead, complexity, latency, and technology. Hence, different works have tackled the problem through a two-time scale approach, e.g., [32], [33], [34]. In light of these considerations, in this paper, we will consider two-timescale solutions that guarantee reliable tracking with significant reduction of RIS reconfiguration rates in the presence of NLOS conditions between the BS and the UE, leveraging the opportunities of near-field propagation.

A. Notation

Scalar variables, vectors, and matrices are represented with lower letters, lower bold letters, and capital bold letters, respectively (e.g., x , \mathbf{x} , and \mathbf{X}). The symbols $(\cdot)^T$, $(\cdot)^H$, and $(\cdot)^{-1}$ represent the transpose, conjugate transpose, and inverse operators of their arguments, respectively. We use t for discrete temporal indexing, i , r for BS and UE antenna indexing, k is the index for indicating a generic RIS and p refers to a single radiating element of a RIS. The notation $\mathbf{x}_{a|b}$ indicates the value of a vector \mathbf{x} at time instant a estimated by considering the measurements collected up to time instant b . For example, $\mathbf{x}_{t|t-1}$ is the value of \mathbf{x} predicted at time instant $t-1$ for the next time instant t , whereas, once a new measurement becomes available at t , this value is updated to $\mathbf{x}_{t|t}$. We denote with $f_{\mathbf{x}}(\mathbf{x})$ the probability density function of the random vector \mathbf{x} , and with $\mathbb{E}_{\mathbf{x}}$ its expectation. The symbol $\Theta = (\theta, \phi)$ includes both the elevation and azimuth angles.

II. MAIN CONTRIBUTIONS

To overcome the limitations present in the literature, in this work, for the first time, we study a two-time scale joint optimization problem for the BS precoder and the RISs reflection coefficients in a single-UE MIMO scenario where a moving UE, either in the far- or near-field, estimates its trajectory using multiple RISs. The main novelty of our work lies in the RIS optimization procedure that is performed to minimize the tracking error in an uncertainty area that accounts for position uncertainty between two subsequent RIS optimization steps. As a result, rather than maximizing the energy towards the instantaneous UE position, as commonly done, the RIS optimization process leads to minimizing the inverse of the received power within the UE uncertainty area. Moreover, differently from the literature, the overall complexity is kept affordable, assuming that RIS optimization is performed less frequently than localization and precoding adaptation. Nonetheless, this

optimization accounts for the trajectory prediction within a finite time horizon, encompassing the period until the next optimization step. This approach avoids the so-called *deafness problem* caused by a loss of tracking due to the narrow beams that would occur using a conventional RIS optimization.

Toward this aim, the main proposed strategies are summarized in the following.

- A novel observation model is introduced for the extended Kalman filter (EKF) tracking process by considering a near-field narrowband signal model and direct positioning. Such an observation model effectively mitigates strong non-linearities caused by phase periodicity, and avoids the synchronization issues without affecting the localization accuracy.
- By leveraging Block Diagonalization (BD) beamforming, we propose a pilot-based precoding method aimed at transmitting separated weighted beams toward the RISs, capable of removing both the cross-RIS interference at the UE and the contribution of the direct BS-UE NLOS connection, notoriously detrimental for localization.
- The joint optimization problem for the transmission parameters based on the definition of the mean squared error (MSE) of the position estimate is recast into a more straightforward form that enables to separate optimization of the RISs phase profiles and the precoders through an iterative block coordinate descent (BCD) algorithm that provides a local optimum. To enable a two-timescale RIS optimization and localization update, the motion model and the UE estimated position are accounted for through a Gaussian Mixture Model-like approach that evaluates the RIS optimization uncertainty area.
- The BS precoders aims at finding the optimal weights for the transmitting beams. Hence, by following the same MSE minimization approach as for RIS optimization, we found that the optimal power allocation for tracking ensures a fair distribution of the power among the different RISs so that the spatial diversity, beneficial for localization, is preserved.

Through the proposed approach, in the numerical results, it is shown that in a typical millimeter-wave indoor scenario, a UE can be tracked with high accuracy with a single BS and few RISs, differently from other existing works that entail the use of many BSs to achieve the 5G positioning requirements. Furthermore, it is confirmed that the conventional strategy of focusing, commonly employed for RIS configuration in the near-field regime, is not the optimal approach for tracking purposes and that the RIS and precoder optimization process tailored for tracking differs from the methods studied in the literature for communication that might lead to suboptimal performance when dealing with UE tracking.

III. PROBLEM FORMULATION AND SYSTEM GEOMETRY

A. Localization Scenario and Geometry

We consider a localization and communication scenario in which a single UE in position $\mathbf{p}_{\text{RX}} \in \mathbb{R}^3$ moves in the environment and localizes itself by processing the received signals

sent by a single BS in $\mathbf{p}_{\text{TX}} \in \mathbb{R}^3$ and reflected by multiple RISs. Either the UE and the BS are equipped with multiple antennas. We denote by $\mathbf{p}_{\text{RX},r} \in \mathbb{R}^3$ and $\mathbf{p}_{\text{TX},i} \in \mathbb{R}^3$, respectively, the positions of the r th antenna on the UE side, with $r \in \mathcal{R} \triangleq \{0, 1, \dots, N_{\text{RX}} - 1\}$, and the i th antenna on the BS side, with $i \in \mathcal{T} \triangleq \{0, 1, \dots, N_{\text{TX}} - 1\}$. In the following, for simplicity, we denote $\mathbf{p}_{\text{RX},0} = \mathbf{p}_{\text{RX}}$ and $\mathbf{p}_{\text{TX},0} = \mathbf{p}_{\text{TX}}$. The considered scenario is also characterized by K large RISs, each of them comprising P unit cells. Consequently each RIS cell position is indicated as $\mathbf{p}_{k,p} \in \mathbb{R}^3$, $k \in \mathcal{K} \triangleq \{1, 2, \dots, K\}$ and $p \in \mathcal{P} \triangleq \{0, 1, \dots, P - 1\}$.

Let define the direction vector as

$$\mathbf{a}(\theta, \phi) = [\sin(\theta) \cos(\phi), \sin(\theta) \sin(\phi), \cos(\theta)]^T, \quad (1)$$

where θ and ϕ are the elevation (measured from the z -axis to the (x, y) -plane) and azimuth (measured from the x -axis) angles. Then, considering the BS as the center of the coordinate system, for each $S \in \{\text{TX}, \text{RX}, k\}$ and for each corresponding antenna index $s \in \{i, r, p\}$, we can indicate the antenna coordinates of each array as

$$\mathbf{p}_{S,s} = [x_{S,s}, y_{S,s}, z_{S,s}]^T = \mathbf{p}_{\text{TX}} + \mathbf{d}_{S,s} \mathbf{a}(\theta_{S,s}, \phi_{S,s}), \quad (2)$$

where $\mathbf{d}_{S,s} = \|\mathbf{p}_{S,s} - \mathbf{p}_{\text{TX}}\|_2$ is the distance from the BS, and $\phi_{S,s} = \text{atan}((y_{S,s} - y_{\text{TX}})/(x_{S,s} - x_{\text{TX}}))$,¹ and $\theta_{S,s} = \text{acos}((z_{S,s} - z_{\text{TX}})/\mathbf{d}_{S,s})$ are the azimuth and elevation angles.² Starting from (2), the distance between the i th antenna of the BS and the p th element of the k th RIS is given by³

$$d_{k,p,i} = \|\mathbf{p}_i - \mathbf{p}_{k,p}\|_2 = \{d_i^2 + d_{k,p}^2 - 2 d_i d_{k,p} [\sin(\theta_i) \cdot \sin(\theta_{k,p}) \cos(\phi_i - \phi_{k,p}) + \cos(\theta_i) \cos(\theta_{k,p})]\}^{1/2} \quad (3)$$

where $\{d_i, \theta_i, \phi_i\}$ are the spherical coordinates of the generic i th transmitting antenna, as defined above. Analogously, we indicate the angle between the i th antenna of the BS and the p th element of the k th RIS as $\Theta_{k,p,i} = (\theta_{k,p,i}, \phi_{k,p,i})$ [20]. $d_{k,r,p}$ and $\Theta_{k,r,p}$ are computed in a similar manner for every k th RIS-UE antenna couple. Next, we consider that the BS and RIS antenna coordinates and array orientation are known. By contrast, the position of the UE is unknown, whereas its orientation is considered known (e.g., estimated by onboard sensors such as compass and gyroscopes [35], [36]). In the numerical results, we will show the impact of orientation residual errors in the system performance. An example of the used localization and communication scenario and its geometry is reported in Fig. 1. From [13], [20] the local reflection coefficient of a unit cell of RIS can be written as $r_{k,r,p,i} = G_c e^{j\Psi_{k,p}} \sqrt{F(\Theta_{k,p,i}) F(\Theta_{k,r,p})}$, where G_c is the gain of the unit-cell and $e^{j\Psi_{k,p}}$ is the phase shift applied to the p th element of the k th RIS. $F(\Theta)$ denotes the normalized power radiation pattern of each unit cell, which is frequency-independent within the bandwidth of interest and

¹The operator atan corresponds to the four-quadrant inverse tangent.

²In the next, the subscripts RX and TX are omitted and $\{\mathbf{p}_r, \mathbf{d}_r, \theta_r, \phi_r\}$ and $\{\mathbf{p}_i, \mathbf{d}_i, \theta_i, \phi_i\}$ are used instead.

³In the sequel, we indicate $d_{\text{RX,TX}} \triangleq \|\mathbf{p}_{\text{RX}} - \mathbf{p}_{\text{TX}}\|$, $d_{r,i} \triangleq \|\mathbf{p}_{\text{RX},r} - \mathbf{p}_{\text{TX},i}\|$, $d_{k,\text{TX}} \triangleq \|\mathbf{p}_k - \mathbf{p}_{\text{TX}}\|$, and $d_{\text{RX},k} \triangleq \|\mathbf{p}_{\text{RX}} - \mathbf{p}_k\|$.

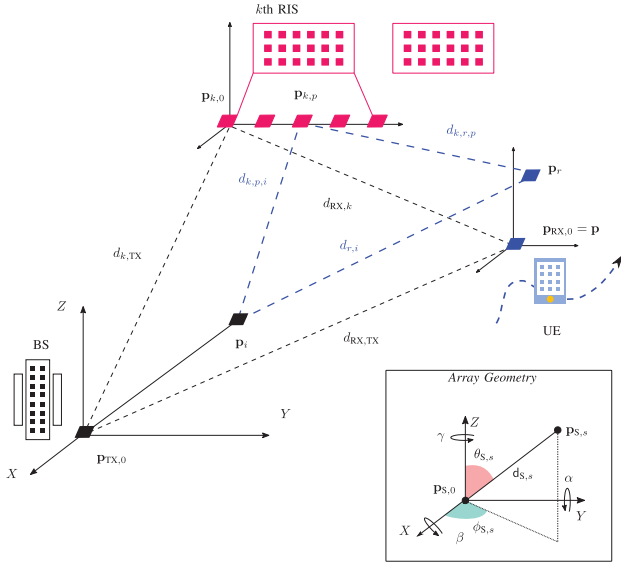


Fig. 1. Joint user tracking and communication scenario.

modeled as an exponential-Lambertian radiation pattern with parameter q as

$$F(\Theta) = \begin{cases} \cos^q(\theta), & \theta \in [0, \pi/2], \phi \in [0, 2\pi] \\ 0, & \text{otherwise} \end{cases} \quad (4)$$

B. Pilot Signal Model

In the following, we describe the proposed pilot-based method for localization and derive the corresponding signal models. The proposed method aims to isolate the contribution of the different RISs at the UE receiver and eliminate the contribution of the direct BS-UE channel since, in many cases, it is a NLOS contribution that does not contain useful information for localization. The BS pilot signal is

$$\mathbf{X} = \mathbf{F} \mathbf{Q} \in \mathbb{C}^{N_{\text{TX}} \times L}, \quad (5)$$

where $\mathbf{Q} = [\mathbf{q}_1, \dots, \mathbf{q}_K]^H \in \mathbb{C}^{K \times L}$ contains K sequences of unitary envelope orthogonal pilot signals, i.e. $|q_{k,l}| = 1$, $\mathbf{q}_k^H \mathbf{q}_m = L \delta_{k,m}$, with $\mathbf{q}_k \in \mathbb{C}^{L \times 1}$, $L \geq K$ being the length of the pilot sequence.⁴ The precoding matrix is indicated as $\mathbf{F} = [\mathbf{f}_1, \dots, \mathbf{f}_K] \in \mathbb{C}^{N_{\text{TX}} \times K}$ and each column $\mathbf{f}_k = \{f_{i,k}\} \in \mathbb{C}^{N_{\text{TX}} \times 1}$, $k \in \mathcal{K}$, is the precoding vector for the k th RIS. The overall received signal at the UE, $\mathbf{Y} \in \mathbb{C}^{N_{\text{RX}} \times L}$, is [11], [20]

$$\mathbf{Y} = \mathbf{H} \mathbf{X} + \sum_{k=1}^K \mathbf{B}_k \mathbf{C}_k \mathbf{G}_k \mathbf{X} + \mathbf{N} \triangleq \mathbf{H} \mathbf{X} + \sum_{k=1}^K \mathbf{Z}_k + \mathbf{N}, \quad (6)$$

where $\mathbf{H} = \{h_{r,i}\} \in \mathbb{C}^{N_{\text{RX}} \times N_{\text{TX}}}$ is the direct BS-UE channel matrix, $\mathbf{B}_k = \{b_{k,r,p}\} \in \mathbb{C}^{N_{\text{RX}} \times P}$ is the channel matrix between the k th RIS and the UE, $\mathbf{G}_k = \{g_{k,p,i}\} \in \mathbb{C}^{P \times N_{\text{TX}}}$ is the channel matrix between the BS and the

⁴More precisely, $L = K$ is the minimum pilot length to obtain orthogonality, although a higher L can also be considered to reduce the overall noise of the received signal at the expense of communication overhead.

k th RIS, $\mathbf{C}_k = \text{diag}(c_{k,1}, \dots, c_{k,p}, \dots, c_{k,P}) = \text{diag}(\mathbf{c}_k) \in \mathbb{C}^{P \times P}$ contains the RISs responses, and $\mathbf{N} \in \mathbb{C}^{N_{\text{RX}} \times L}$ represents the additive white Gaussian noise sequences with variance σ^2 . For the communication system, it is assumed $N_{\text{TX}} \geq N_{\text{RX}}$. The generic RIS coefficient $\{c_{k,p}\}$, $p \in \mathcal{P}$, $k \in \mathcal{K}$, denotes the normalized reflection coefficient of the p th element of the k th RIS, i.e., $c_{k,p} = e^{j\psi_{k,p}}$. Hence, the channel components are modeled as

$$h_{r,i} = \sqrt{\frac{\kappa_h}{\kappa_h + 1}} \gamma_{r,i} e^{-j\frac{2\pi}{\lambda} d_{r,i}} + \sqrt{\frac{1}{\kappa_h + 1}} \beta_{r,i}, \quad (7)$$

$$g_{k,p,i} = \rho_{k,p,i} e^{-j\frac{2\pi}{\lambda} d_{k,p,i}}, \quad (8)$$

$$b_{k,r,p} = \sqrt{\frac{\kappa_b}{\kappa_b + 1}} \rho_{k,r,p} e^{-j\frac{2\pi}{\lambda} d_{k,r,p}} + \sqrt{\frac{1}{\kappa_b + 1}} \alpha_{k,r,p}, \quad (9)$$

where $\gamma_{r,i} \triangleq \frac{\lambda}{4\pi} \frac{\sqrt{G_i G_r}}{d_{\text{RX},\text{TX}}}$, $\rho_{k,p,i} \triangleq \frac{\lambda}{4\pi} \frac{\sqrt{G_i G_c F(\Theta_{k,p,i})}}{d_{k,\text{TX}}}$, $\rho_{k,r,p} \triangleq \frac{\lambda}{4\pi} \frac{\sqrt{G_r G_c F(\Theta_{k,r,p})}}{d_{\text{RX},k}}$ are the channel amplitude of the line-of-sight (LOS) components, $\kappa_h \geq 0$ and $\kappa_b \geq 0$ are the Ricean factors for the direct BS-UE and RIS-UE links, respectively, $\alpha_{k,r,p} \sim \mathcal{CN}(0, \rho_{k,r,p}^2)$ and $\beta_{r,i} \sim \mathcal{CN}(0, \gamma_{r,i}^2)$ denote the random complex fading coefficients of the NLOS component [37]. $\rho_{k,r,p}$, $\rho_{k,p,i}$, and $\gamma_{r,i}$ represent the compact notation of the amplitude channel coefficients (except for the Ricean factor terms), λ is the wavelength, G_i is the gain of a single antenna element from BS, G_r is the gain of a single antenna element from UE, and G_c is the gain of a RIS unit cell.⁵ In accordance to [38], we assume a LOS channel between the BS and the RIS which is a realistic condition of most practical scenarios. The received signal is then projected over each pilot sequence \mathbf{q}_k to get the contribution of the k th RIS, as

$$\begin{aligned} \mathbf{y}_k &= \frac{1}{L} \mathbf{Y} \mathbf{q}_k = \sum_{l=1}^K \mathbf{B}_l \mathbf{C}_l \mathbf{G}_l \mathbf{f}_k + \mathbf{H} \mathbf{f}_k + \frac{1}{L} \mathbf{N} \mathbf{q}_k \\ &= \mathbf{z}_k + \mathbf{n}_k \in \mathbb{C}^{N_{\text{RX}} \times 1}, \end{aligned} \quad (10)$$

where $\mathbf{z}_k \triangleq \mathbf{B}_k \mathbf{C}_k \mathbf{G}_k \mathbf{f}_k$ represents the useful part of the received signal with respect to the k th RIS, $\mathbf{n}_k = \sum_{l=1, l \neq k}^K \mathbf{z}_l + \mathbf{H} \mathbf{f}_k + \mathbf{n}'_k$ is the noise plus interference terms, and $\mathbf{n}'_k \triangleq \frac{1}{L} \mathbf{N} \mathbf{q}_k$ is the AWGN noise term after correlation with the pilot sequence where each element has a power of σ^2/L , with L being the pilot sequence length.

C. Block Diagonalization Precoding

The goal of the proposed precoding strategy is to maximize the received energy while eliminating interference to the k th received signal in (10) due to the presence of the direct BS-UE channel and the other RISs.⁶ In this case, $\sum_{l=1, l \neq k}^K \mathbf{z}_l \simeq 0$ and

⁵According to the observation model entailed for this work (see Section IV-B) we can directly neglect BS-UE synchronization errors since they will not influence the algorithm performance.

⁶This goal can be achieved by placing the RISs at a certain height above the ground and at a sufficient distance from each other so that they receive energy only from the intended beam. Optimal RISs placement is beyond the scope of this work and has already been studied in [10], [39] for localization-based applications. In our settings, RIS placement for simulations is chosen to ensure model assumptions.

$\mathbf{H}\mathbf{f}_k \simeq 0$. Indeed, NLOS conditions occur frequently in the direct BS-UE link in practical wireless communication scenarios. Moreover, this is the situation where the RISs can provide the greatest benefits. Therefore, in our work, we assume that the LOS component of the BS-UE signal is blocked, i.e., the BS-UE link only results in NLOS propagation, which is not useful for localization. Under these NLOS conditions, localization is indeed very difficult and subject to serious errors, [40], [41], and therefore the direct BS-UE connection is not considered in our localization scheme. Given a scenario with multiple antennas on the BS, this condition can be exactly satisfied by using BD beamforming. This procedure, commonly used to suppress interference between different UEs [42], aims to orthogonalize the available channels by projecting the transmitted signal for the k th RIS into the null space of its interference. To elaborate, we introduce the k th RIS interference channel matrix $\tilde{\mathbf{G}}_k \in \mathbb{C}^{\tilde{\alpha} \times N_{\text{TX}}}$ as

$$\tilde{\mathbf{G}}_k = [\mathbf{G}_1^T, \dots, \mathbf{G}_{k-1}^T, \mathbf{G}_{k+1}^T, \dots, \mathbf{G}_K^T, \mathbf{H}^T]^T, \quad (11)$$

with $\tilde{\alpha} = N_{\text{RX}} + (K-1)P$. Applying the Singular Value Decomposition (SVD) it is possible to rewrite the matrix as

$$\tilde{\mathbf{G}}_k = \tilde{\mathbf{U}}_k \tilde{\mathbf{\Lambda}}_k \tilde{\mathbf{V}}_k^H. \quad (12)$$

Denoting by $\tilde{p} \triangleq \text{rank}(\tilde{\mathbf{\Lambda}}_k)$, we can write $\tilde{\mathbf{V}}_k = [\tilde{\mathbf{V}}_k^{(1)}, \tilde{\mathbf{V}}_k^{(0)}]$, where $\tilde{\mathbf{V}}_k^{(1)} \in \mathbb{C}^{N_{\text{TX}} \times \tilde{p}}$ and $\tilde{\mathbf{V}}_k^{(0)} \in \mathbb{C}^{N_{\text{TX}} \times N_{\text{TX}} - \tilde{p}}$ spans the null space of $\tilde{\mathbf{G}}_k$. Specifically, the precoding vector \mathbf{f}_k is designed as $\mathbf{f}_k = \tilde{\mathbf{V}}_k^{(0)} \tilde{\mathbf{f}}_k$ such that $\mathbf{G}_l \mathbf{f}_k = \mathbf{0}$, for $l \neq k$ and $\mathbf{H}\mathbf{f}_k = \mathbf{0}$, i.e., the inter-RIS and direct link interferences are completely removed in (10). As for $\tilde{\mathbf{f}}_k$, it represents the precoding vector of an equivalent MIMO channel with $N_{\text{TX}} - \tilde{p}$ antennas, transmitting over the equivalent channel $\tilde{\mathbf{G}}_k = \mathbf{G}_k \tilde{\mathbf{V}}_k^{(0)} \in \mathbb{C}^{P \times (N_{\text{TX}} - \tilde{p})}$, and can be designed by classical beamforming techniques. To elaborate, we denote by $\tilde{\mathbf{v}}_k^{(0)}$ the first right singular vector of the SVD decomposition of $\tilde{\mathbf{G}}_k$, which corresponds to its optimal beamforming vector. The normalized beamforming vector $\mathbf{v}_k^{(0)}$ for \mathbf{G}_k can be expressed as follows

$$\mathbf{v}_k^{(0)} = \tilde{\mathbf{V}}_k^{(0)} \tilde{\mathbf{v}}_k^{(0)} / \|\tilde{\mathbf{V}}_k^{(0)} \tilde{\mathbf{v}}_k^{(0)}\|. \quad (13)$$

Thus, if we denote by β_k^2 the power budget allocated at the BS for the k th RIS, we have

$$\mathbf{f}_k = \beta_k \mathbf{v}_k^{(0)}. \quad (14)$$

It is worth noting that the BD method reduces the number of equivalent antennas available at the BS for each RIS, thus, limiting the beamforming gain. However, if the RISs are at a certain height and sufficiently spaced, this effect may be negligible. As a result of the interference elimination, the received signal from the k th RIS can be expressed as

$$y_{k,r} = \sqrt{\frac{\kappa_b}{\kappa_b + 1}} \sum_{i=0}^{N_{\text{TX}}-1} f_{i,k} \sum_{p=0}^{P-1} \rho_{k,p,i} \rho_{k,r,p} c_{k,p} e^{-j\frac{2\pi}{\lambda} d_{k,r,p,i}} + n_{k,r} = a_{k,r} + n_{k,r}, \quad (15)$$

with $d_{k,r,p,i} \triangleq d_{k,p,i} + d_{k,r,p}$. The noise $n_{k,r}$ includes the AWGN noise and the multipath components after

correlation with the pilot signal and can be expressed as $n_{k,r} \sim \mathcal{CN}(0, \sigma_{k,r}^2) = \mathcal{CN}\left(0, \frac{\sigma^2}{L} + \frac{1}{\kappa_b + 1} \sum_{p=0}^{P-1} \rho_{k,r,p}^2\right)$. In most practical situations, the dimension of the UE antenna system is small compared to the distance to the RIS, we can assume that the same power is received at the different UE antennas, i.e., $\rho_{k,r,p} = \rho_{k,p}$, $\forall r \in \mathcal{R}$. Accordingly, we have the same noise variance at the different antennas, i.e., $n_{k,r} \sim \mathcal{CN}(0, \sigma_k^2)$.

IV. BAYESIAN USER TRACKING

We now consider a single UE tracking problem in SREs where localization is aided by the presence of multiple RISs. A common representation for tracking systems is a state-space model [43] consisting of a *transition model* that describes the evolution of the state over time and an *observation model* that specifies how the measurements are related to the UE state. In mathematical terms, we have

$$\mathbf{s}_t = f(\mathbf{s}_{t-1}) + \mathbf{w}_t, \quad (16)$$

$$\mathbf{o}_t = h(\mathbf{s}_t) + \boldsymbol{\eta}_t, \quad (17)$$

where $\mathbf{s}_t \triangleq [\mathbf{p}_t, \dot{\mathbf{p}}_t] \in \mathbb{R}^{N_s}$ is the state vector at time instant t and contains the position (\mathbf{p}_{RX}) and velocity ($\dot{\mathbf{p}}_{\text{RX}}$) of the UE at time t , and N_s is the dimension of the state vector. The transition function is indicated as $f(\mathbf{s}_{t-1})$ (in the following, a linear function is assumed as $f(\mathbf{s}_{t-1}) = \mathbf{T} \mathbf{s}_{t-1}$), and \mathbf{o}_t is the observation model with $h(\mathbf{s}_t)$ as the observation function. \mathbf{w}_t and $\boldsymbol{\eta}_t$ are stochastic Gaussian noise processes.

A. Transition Model

For the transition model, we consider a second-order kinematic model [44]

$$\mathbf{T} = \begin{bmatrix} \mathbf{I}_3 & dt \mathbf{I}_3 \\ \mathbf{0}_3 & \mathbf{I}_3 \end{bmatrix}, \quad \mathbf{w}_t \sim \mathcal{N}(\mathbf{w}_t; \mathbf{0}, \mathbf{P}), \quad \mathbf{P} = \begin{bmatrix} \frac{dt^3}{3} \mathbf{P}_a & \frac{dt^2}{2} \mathbf{P}_a \\ \frac{dt^2}{2} \mathbf{P}_a & dt \mathbf{P}_a \end{bmatrix}, \quad (18)$$

where dt is the delay between two adjacent time instants t and $t+1$, and $\mathbf{P}_a = \text{diag}(\sigma_{a,x}^2, \sigma_{a,y}^2, \sigma_{a,z}^2)$ [45].

B. Observation Model

In MIMO systems, different signal parameters are considered to retrieve the location information [11], [43]. In the presence of wideband signals, time-of-arrival (TOA) and AOA can be used together to allow positioning [46], while with narrowband signals and multiple antennas, AOAs can be extrapolated from the signal phases in far-field conditions [17]. When operating in the near-field region, the phases of narrowband signals embody richer information by also depending on ranging [14], [45].

Such approaches, that first derive the geometric signal parameters and then estimate the position starting from them, are referred to as two-step techniques. Two-step approaches are generally suboptimal compared to direct methods that start from the received signal and avoid intermediate processing steps

[13]. In addition, modeling the measurement noise in the two-step approach could be a difficult task due to the nonlinear operations, which is avoided when starting directly from the received signals whose statistics are known [15], [16]. Therefore, in our narrowband method, we opt for a direct approach, where the range and angle information is implicitly accounted for by processing the received signals.

Consequently, to define the observation vector, we denote the normalized received signals under the assumption of high signal-to-noise ratio (SNR) as

$$\bar{y}_{k,r} = \frac{y_{k,r}}{|y_{k,r}|} \approx \frac{a_{k,r} + n_{k,r}}{|a_k|} = \bar{a}_{k,r} + \bar{n}_{k,r}, \quad (19)$$

where in (19) we have exploited the assumption of equal power at the different UE antennas, leading to $|a_{k,r}| = |a_k|$, and introduced the normalized useful term $\bar{a}_{k,r} = \frac{a_{k,r}}{|a_k|}$.⁷ For the noise term we have $\bar{n}_{k,r} \sim \mathcal{CN}(0, \bar{\sigma}_k^2)$ with

$$\bar{\sigma}_k^2 \simeq \frac{\sigma_k^2}{|a_k|^2}. \quad (20)$$

Starting from the normalized received signals in (19), without approximation, we consider the correlation between measurements at adjacent antennas as observations. In particular, for $Z = \lfloor N_{\text{RX}}/2 \rfloor$, the observation vector is given by

$$\mathbf{o}_t \triangleq [\Re\{\chi_1\}, \dots, \Re\{\chi_k\}, \dots, \Re\{\chi_K\}, \Im\{\chi_1\}, \dots, \Im\{\chi_k\}, \dots, \Im\{\chi_K\}] \in \mathbb{R}^{2KZ}, \quad (21)$$

where the generic term $\chi_k = \{\chi_{k,\tilde{r}}\}$, $\tilde{r} \in \mathcal{Z} \triangleq \{0, 1, \dots, Z-1\}$, is a phase gradient given by

$$\chi_{k,\tilde{r}} = (\bar{y}_{k,2\tilde{r}+1}) (\bar{y}_{k,2\tilde{r}})^* \quad (22)$$

in which the dependence on the UE state \mathbf{s} is implicit in the received signal's phase term. When operating within the radiating near-field domain, (22) contains both range and bearing information (as it can also be seen from the system geometry of (3)), while in the far-field, it contains only AOA information [45]. Moreover, by directly processing the received signals, it is possible to fit the Gaussian model for the observation noise underlying the implementation of KF, differently from what happens when considering the statistics of a specific estimator for AOA.

Another advantage of considering the gradient in (22) is the possibility of avoiding strong non-linearities arising from fast variations of the observed signals along the antenna array, which could undermine the functioning of the tracking algorithm considered in this paper. More precisely, (22) is used to achieve a double effect. On the one hand, normalizing the received signal (i.e., using $\bar{y}_{k,2\tilde{r}}$ instead of $y_{k,2\tilde{r}}$) allows the observations to be independent of the received powers, which contain information about the distance but can vary rapidly due to the ability of RISs to form very narrow beams.

⁷This assumption allows us to simplify the derivation of a tractable observation model to use in the EKF. However, the measurements generated for the simulations were derived from the actual observed signal, i.e., $\bar{y}_{k,r} = \frac{y_{k,r}}{|y_{k,r}|}$, without any approximation. Subsequently, simulation results confirmed that this model mismatch does not significantly degrade performance.

Moreover, received signal strength (RSS) measurements lead to less accurate positioning with respect to TOA or AOA measurements [11]. On the other hand, conjugate multiplication (i.e., $\bar{y}_{k,2\tilde{r}+1} \bar{y}_{k,2\tilde{r}}^*$ instead of $\bar{y}_{k,2\tilde{r}+1}$ alone) allows getting rid of the dependence on absolute phase, which is also rapidly variable and affected by possible clock offsets deriving from synchronization errors. Practically, using the phase differences instead of the absolute phases does not mean losing important information.

The observation function in (17) is given by the expected mean of (21), i.e., $h(\mathbf{s}_t) \triangleq \mathbb{E}[\mathbf{o}_t]$, whose generic elements can be easily computed as

$$h(\Re\{\chi_{k,\tilde{r}}\}) = \mathbb{E}\{\Re\{\chi_{k,\tilde{r}}\}\} = \Re\{\bar{a}_{k,2\tilde{r}+1} \bar{a}_{k,2\tilde{r}}^*\} \quad (23)$$

$$h(\Im\{\chi_{k,\tilde{r}}\}) = \mathbb{E}\{\Im\{\chi_{k,\tilde{r}}\}\} = \Im\{\bar{a}_{k,2\tilde{r}+1} \bar{a}_{k,2\tilde{r}}^*\}. \quad (24)$$

The measurement noise $\boldsymbol{\eta}_t$ of (17) is considered as zero-mean Gaussian distributed noise with a diagonal covariance matrix \mathbf{R}_t . Now consider $\{\mathbf{R}_t\}_{n,n}$ the n th element of the main diagonal of \mathbf{R}_t , and denote by $\mathcal{I}_k = \{(k-1)Z + \tilde{r} + (m-1)KZ + 1\}$, for $\tilde{r} \in \mathcal{Z}$, $m = 1, 2$, the set of indices of the observation vectors corresponding to the signal received from the k th RIS. Thus, considering a general $n \in \mathcal{I}_k$ and for each $\tilde{r} \in \mathcal{Z}$, we have

$$\begin{aligned} \{\mathbf{R}_t\}_{n,n} &= \text{var}\{\Re\{\chi_{k,\tilde{r}}\}\} = \text{var}\{\Im\{\chi_{k,\tilde{r}}\}\} \\ &\approx \text{var}\{\Re(\bar{a}_{k,2\tilde{r}+1}) \Re(\bar{n}_{k,2\tilde{r}}) + \Im(\bar{a}_{k,2\tilde{r}+1}) \Im(\bar{n}_{k,2\tilde{r}}) \\ &\quad + \Re(\bar{a}_{k,2\tilde{r}}) \Re(\bar{n}_{k,2\tilde{r}+1}) + \Im(\bar{a}_{k,2\tilde{r}}) \Im(\bar{n}_{k,2\tilde{r}+1})\} \\ &= \frac{\bar{\sigma}_k^2}{2} [|\bar{a}_k|^2] + \frac{\bar{\sigma}_k^2}{2} [|\bar{a}_k|^2] = \bar{\sigma}_k^2 = \frac{\sigma_k^2}{|a_k|^2} \end{aligned} \quad (25)$$

where, as before, we assume a large SNR regime and independence between the received signals at adjacent antennas. In words, \mathbf{R}_t has a blockwise diagonal structure in which all elements corresponding to the signal received from the k th RIS have the same value $\bar{\sigma}_k^2$.

C. EKF Algorithm

Among the Bayesian estimators, we use the extended Kalman filter (EKF). The state is described by a Gaussian distribution $\mathbf{s}_t \sim \mathcal{N}(\mathbf{s}_t; \mathbf{m}_{t|t}, \boldsymbol{\Sigma}_{t|t})$, where $\mathbf{m}_{t|t} \in \mathbb{R}^{N_s}$ and $\boldsymbol{\Sigma}_{t|t} \in \mathbb{R}^{N_s^2}$ are the posterior mean vector and the covariance matrix of the state. An important step of the EKF is the evaluation of the Jacobian matrix, associated with the linearization of the observation model $h(\mathbf{s}_t)$, and written as $\mathbf{J}_t \triangleq \nabla_{\mathbf{s}_t} h(\mathbf{s}_t)$, where $\nabla_{\mathbf{s}_t}$ is the gradient with respect to the state vector. The Jacobian is evaluated at $\mathbf{s}_t = \mathbf{m}_{t|t-1}$, where $\mathbf{m}_{t|t-1}$ is the predicted state (for $t = 1$ it is $\mathbf{m}_{t|t-1} = \mathbf{m}_0$). The Jacobian computation is reported in the supplementary material as Appendix A, whereas the EKF is reported in Algorithm 1, in which $\boldsymbol{\vartheta}_k^{(t)}$ represents the transmission parameters to be optimized at time t and for the k th RIS (see Sec. V).

Noise Covariance Computation: Calculating \mathbf{R}_t in (25) to be plugged into the EKF is problematic because $\bar{\sigma}_k^2$ depends on the multipath, which is difficult to predict, and $|a_k|^2$ depends on the UE's location, which is the unknown term that must

Algorithm 1: Extended Kalman Filter**Initialization for $t = 0$:**

- Initialize the state $\mathbf{s}_0 \sim \mathcal{N}(\mathbf{s}_0; \mathbf{m}_0, \Sigma_0)$;
- Initialize the transmission parameters $\boldsymbol{\vartheta}_k^{(1)} = (\mathbf{c}_k^{(1)}, \beta_k^{(1)})$ for $k = 1, \dots, K$;
- Set $\mathbf{m}_{1|0} = \mathbf{m}_0$, $\Sigma_{1|0} = \Sigma_0$, $\mathbf{h}_{1|0} = h(\mathbf{m}_{1|0})$;

for $t = 1, \dots, T$ do**Measurement update;**

- Collect a new measurement vector \mathbf{o}_t ;
- Compute the innovation:
 $\mathbf{v}_t = \mathbf{o}_t - \mathbf{h}_{t|t-1}$;
- Compute the Kalman gain:
 $\mathbf{S}_{t|t-1} = \mathbf{J}_t \Sigma_{t|t-1} \mathbf{J}_t^T + \mathbf{R}_t$;
- Update the posterior state estimate and covariance:
 $\mathbf{K}_t = \Sigma_{t|t-1} \mathbf{J}_t^T \mathbf{S}_{t|t-1}^{-1}$;

$$\mathbf{m}_{t|t} = \mathbf{m}_{t|t-1} + \mathbf{K}_t \mathbf{v}_t;$$

$$\Sigma_{t|t} = \Sigma_{t|t-1} - \mathbf{K}_t \mathbf{S}_{t|t-1} \mathbf{K}_t^T;$$

State Estimation;

- Estimate the state:

$$\hat{\mathbf{s}}_t = \mathbf{m}_{t|t};$$

Time Update: State Prediction and RIS**Optimization;**

- Predict the a-priori moments of the state based on the previous a-posteriori estimates;

$$\mathbf{m}_{t+1|t} = \mathbf{T} \mathbf{m}_{t|t};$$

$$\Sigma_{t+1|t} = \mathbf{T} \Sigma_{t|t} \mathbf{T}^T + \mathbf{P};$$

$$\text{Evaluate } \mathbf{J}_{t+1} \text{ and } \mathbf{h}_{t+1|t} = h(\mathbf{m}_{t+1|t});$$

- Calculate $\boldsymbol{\vartheta}_k^{(t+1)} = (\mathbf{c}_k^{(t+1)}, \beta_k^{(t+1)})$ for $k = 1, \dots, K$ (see Algorithm 2 and 3).

end

be estimated. To circumvent this difficulty, we consider an approximation for \mathbf{R}_t called $\tilde{\mathbf{R}}_t$, where

$$\left\{ \tilde{\mathbf{R}}_t \right\}_{n,n} = \frac{\sigma^2(1+\alpha)}{\|\mathbf{y}_k\|^2/N_{\text{RX}}}, \quad (26)$$

for $n \in \mathcal{I}_k$. In (26) $\|\mathbf{y}_k\|^2/N_{\text{RX}}$ is the average received power measured at the receiver, and α is an empirical parameter introduced to oversize the variance of the noise in the observation model with respect to the expected value to account for the noise increase due to multipath.⁸

V. RIS AND PRECODER OPTIMIZATION FOR USER TRACKING: PROBLEM FORMULATION

In this section, we will introduce a joint optimization problem to design the transmission parameters, that is, the precoding vectors and the RISs reflection coefficients. At time t and for the k th RIS, these parameters are grouped in a vector given by

$$\boldsymbol{\vartheta}_k^{(t)} = (\mathbf{c}_k^{(t)}, \beta_k^{(t)}). \quad (27)$$

The vector includes $\mathbf{c}_k^{(t)}$, that contains the k th RIS reflection coefficients, and $\beta_k^{(t)}$, the real-valued weights that determine the

⁸This is the typical approach followed in the literature to account for potential model mismatch in the observation that might be caused, for instance, by fading [47].

amount of power to be assigned to the k th RIS. The constraint on the power allocation is given by $\sum_{k=1}^K (\beta_k^{(t)})^2 = P_{\text{tx}}$, with P_{tx} denoting the power budget provided for the transmission from the BS to the K RISs. As illustrated in Section III-C, the precoding vector can be found using a BD approach so that the overall precoding optimization problem turns out to be a power allocation problem to different RISs, i.e., $\mathbf{f}_k^{(t)} = \beta_k^{(t)} \mathbf{v}_k^{(0)}$.

The optimization of parameters in (27) is performed during the time update stage of the EKF, where we predict the state and covariance for the next time step $t+1$ with the availability of measurements up to time t . Such measurements and information consist of \mathbf{J}_{t+1} , $\mathbf{m}_{t+1|t}$, and $\Sigma_{t+1|t}$, among others (see Algorithm 1).

A. Cost Function

To define a cost function for optimizing the transmission parameters at time t , it is natural to consider the covariance matrix of the state at the next time, \mathbf{s}_{t+1} . However, note that the expression of the covariance matrix $\Sigma_{t+1|t+1}$ of the EKF used in Algorithm 1 depends on \mathbf{R}_{t+1} , which in turn depends on the position \mathbf{p}_{t+1} , not yet available. Therefore, $\Sigma_{t+1|t+1}$ in Algorithm 1 cannot be used for our purposes. Indeed, recalling (20) and assuming the same empirical term α introduced in (26) to characterize the observation model mismatch, the covariance matrix of $\boldsymbol{\eta}_{t+1}$ is given by

$$\begin{aligned} [\mathbb{E} \{ \boldsymbol{\eta}_{t+1} \boldsymbol{\eta}_{t+1}^T \}]_{n,n} &= \left[\mathbf{R}_{t+1} \left(\mathbf{s}_{t+1}, \boldsymbol{\vartheta}^{(t+1)} \right) \right]_{n,n} \\ &= \bar{\sigma}_k^2 = \frac{\sigma^2(1+\alpha)}{P_k(\mathbf{p}_{t+1}, \boldsymbol{\vartheta}^{(t+1)})} \end{aligned} \quad (28)$$

with $n \in \mathcal{I}_k$, $\boldsymbol{\vartheta}^{(t+1)} = \{ \boldsymbol{\vartheta}_1^{(t+1)}, \dots, \boldsymbol{\vartheta}_K^{(t+1)} \}$, and $P_k(\mathbf{p}_{t+1}, \boldsymbol{\vartheta}^{(t+1)})$ representing the power received by the k -th RIS when the node is at position \mathbf{p}_{t+1} for a determined $\boldsymbol{\vartheta}_k^{(t+1)}$. It is also worth noting that the error covariance matrix in (28) does not depend on velocity, so we can simplify as $\mathbf{R}_{t+1}(\mathbf{s}_{t+1}, \boldsymbol{\vartheta}^{(t+1)}) = \mathbf{R}_{t+1}(\mathbf{p}_{t+1}, \boldsymbol{\vartheta}^{(t+1)})$.

This being the case, to circumvent this problem, we derive a new cost function that can be evaluated at time t , with the goal of minimizing the MSE of the UE state estimate for the next time. To simplify the notation in the following, the temporal index $t+1$ is omitted from the parameters $(\mathbf{p}_{t+1}, \boldsymbol{\vartheta}^{(t+1)})$, i.e., $(\mathbf{p}, \boldsymbol{\vartheta})$ is used instead. Let us now denote

$$\mathbf{S}_{t+1}(\mathbf{p}, \boldsymbol{\vartheta}) = \mathbf{J}_{t+1} \Sigma_{t+1|t} \mathbf{J}_{t+1}^T + \mathbf{R}_{t+1}(\mathbf{p}, \boldsymbol{\vartheta}), \quad (29)$$

$$\mathbf{K}_{t+1}(\mathbf{p}, \boldsymbol{\vartheta}) = \Sigma_{t+1|t} \mathbf{J}_{t+1}^T \mathbf{S}_{t+1}^{-1}(\mathbf{p}, \boldsymbol{\vartheta}). \quad (30)$$

The state estimate at time $t+1$ is

$$\hat{\mathbf{s}}_{t+1} = \mathbf{m}_{t+1|t+1} = \mathbf{m}_{t+1|t} + \mathbf{K}_{t+1}(\mathbf{p}, \boldsymbol{\vartheta}) \mathbf{v}_{t+1}, \quad (31)$$

with the innovation vector given by

$$\mathbf{v}_{t+1} = \mathbf{o}_{t+1} - \mathbf{h}_{t+1|t} = \mathbf{J}_{t+1} (\mathbf{s}_{t+1} - \mathbf{m}_{t+1|t}) + \boldsymbol{\eta}_{t+1}. \quad (32)$$

In the given expression $\mathbf{h}_{t+1|t}$ is the observation function evaluated in $\mathbf{m}_{t+1|t}$, i.e., $\mathbf{h}_{t+1|t} = h(\mathbf{m}_{t+1|t})$, \mathbf{J}_{t+1} is the Jacobian matrix evaluated in $\mathbf{m}_{t+1|t}$ and \mathbf{o}_{t+1} is the observation signal in the next time instant position \mathbf{p}_{t+1} . Note that (32) is the

linearized version of (17) according to the first-order Taylor expansion. Under these circumstances, we can condition on the future state \mathbf{s}_{t+1} and introduce the cost function as follows

$$\begin{aligned} \mathcal{E}(\mathbf{p}, \boldsymbol{\vartheta}) &= \text{Tr} \left(\mathbb{E}_{\eta_{t+1}} \left\{ (\mathbf{s}_{t+1} - \hat{\mathbf{s}}_{t+1}) (\mathbf{s}_{t+1} - \hat{\mathbf{s}}_{t+1})^T \right\} \right) \\ &= \text{Tr} \left(\mathbb{E}_{\eta_{t+1}} \left\{ (\Delta \mathbf{s}_{t+1} - \mathbf{K}_{t+1}(\mathbf{p}, \boldsymbol{\vartheta}) \mathbf{v}_{t+1}) \cdot \right. \right. \\ &\quad \left. \left. \times (\Delta \mathbf{s}_{t+1} - \mathbf{K}_{t+1}(\mathbf{p}, \boldsymbol{\vartheta}) \mathbf{v}_{t+1})^T \right\} \right), \quad (33) \end{aligned}$$

where $\text{Tr}(\cdot)$ is the trace operator, $\mathbb{E}_{\eta_{t+1}}\{\cdot\}$ is the expected value evaluated with respect to the observation noise and $\Delta \mathbf{s}_{t+1} = (\mathbf{s}_{t+1} - \mathbf{m}_{t+1|t})$ is an unknown random variable depending on the future state.

From (28)–(32) we obtain the following

$$\mathbb{E}_{\eta_{t+1}} \left\{ \mathbf{v}_{t+1} \mathbf{v}_{t+1}^T \right\} = \mathbf{J}_{t+1} \Delta \mathbf{s}_{t+1} \Delta \mathbf{s}_{t+1}^T \mathbf{J}_{t+1}^T + \mathbf{R}_{t+1}(\mathbf{p}, \boldsymbol{\vartheta}), \quad (34)$$

$$\mathbb{E}_{\eta_{t+1}} \left\{ \mathbf{v}_{t+1} \Delta \mathbf{s}_{t+1}^T \right\} = \mathbf{J}_{t+1} (\Delta \mathbf{s}_{t+1} \Delta \mathbf{s}_{t+1}^T), \quad (35)$$

and it is easy to reformulate (33) as

$$\begin{aligned} \mathcal{E}(\mathbf{p}, \boldsymbol{\vartheta}) &= \text{Tr} \left(\Delta \mathbf{s}_{t+1} \Delta \mathbf{s}_{t+1}^T - \mathbf{K}_{t+1}(\mathbf{p}, \boldsymbol{\vartheta}) \mathbf{J}_{t+1} \Delta \mathbf{s}_{t+1} \Delta \mathbf{s}_{t+1}^T \right. \\ &\quad \left. - \Delta \mathbf{s}_{t+1} \Delta \mathbf{s}_{t+1}^T \mathbf{J}_{t+1}^T \mathbf{K}_{t+1}(\mathbf{p}, \boldsymbol{\vartheta})^T \right. \\ &\quad \left. + \mathbf{K}_{t+1}(\mathbf{p}, \boldsymbol{\vartheta}) \left[\mathbf{J}_{t+1} \Delta \mathbf{s}_{t+1} \Delta \mathbf{s}_{t+1}^T \mathbf{J}_{t+1}^T \right. \right. \\ &\quad \left. \left. + \mathbf{R}_{t+1}(\mathbf{p}, \boldsymbol{\vartheta}) \right] \mathbf{K}_{t+1}(\mathbf{p}, \boldsymbol{\vartheta}) \right). \quad (36) \end{aligned}$$

B. Problem Formulation

We are now in a position to define the optimization problem at hand, i.e.:

$$\begin{aligned} \min_{\boldsymbol{\vartheta}} \mathbb{E}_{\mathbf{s}_{t+1|t}} \{ \mathcal{E}(\mathbf{p}, \boldsymbol{\vartheta}) \} \\ \text{s.t. } \boldsymbol{\vartheta} \in \mathcal{Q} \end{aligned}, \quad (37)$$

where $\mathbb{E}_{\mathbf{s}_{t+1|t}}$ is the average over $\mathbf{s}_{t+1|t} \sim \mathcal{N}(\mathbf{m}_{t+1|t}, \boldsymbol{\Sigma}_{t+1|t})$ and \mathcal{Q} includes the precoder and RISs constraints, i.e., $\sum_{k=1}^K \beta_k^2 \leq P_{\text{tx}}$, $|c_{k,p}| \leq 1, \forall k \in \mathcal{K}, p \in \mathcal{P}$. Since $\mathbb{E}_{\mathbf{s}_{t+1|t}} \{ \Delta \mathbf{s}_{t+1} \Delta \mathbf{s}_{t+1}^T \} = \boldsymbol{\Sigma}_{t+1|t}$, it is easy to verify that if we replace \mathbf{p} in (36) with the actual UE position, then $\mathbb{E}_{\mathbf{s}_{t+1|t}} \{ \mathcal{E}(\mathbf{p}, \boldsymbol{\vartheta}) \} = \text{Tr}(\boldsymbol{\Sigma}_{t+1|t+1})$ [48]. Thus, the problem considered consists in minimizing the average of the trace of the covariance matrix of \mathbf{s}_{t+1} , based on observations at time t . However, the computation of the expected value with respect to the position in (36) is very complex, given the inverse proportionality of $\mathbf{R}_{t+1}(\mathbf{p}, \boldsymbol{\vartheta})$ in $\mathbf{K}_{t+1}(\mathbf{p}, \boldsymbol{\vartheta})$. As such, in order to reduce the computational complexity of the problem, the idea could be to introduce a fixed Kalman gain matrix $\tilde{\mathbf{K}}_{t+1}$ that does not depend on the error covariance matrix $\mathbf{R}_{t+1}(\mathbf{p}, \boldsymbol{\vartheta})$ but is expressed in terms of an approximation for the covariance matrix, fixed and independent of the transmission parameters. Accordingly we consider $\tilde{\mathbf{K}}_{t+1}$ to be used in (37) as

$$\tilde{\mathbf{K}}_{t+1} = \boldsymbol{\Sigma}_{t+1|t} \mathbf{J}_{t+1}^T \left(\mathbf{J}_{t+1} \boldsymbol{\Sigma}_{t+1|t} \mathbf{J}_{t+1}^T + \check{\mathbf{R}}_t \right)^{-1}, \quad (38)$$

where $\check{\mathbf{R}}_t$ is an estimate at time t of the noise covariance matrix at time $t+1$. To evaluate $\check{\mathbf{R}}_t$, the working principle of our

approach is exploited for the optimization algorithm. Due to the power balancing effect introduced by the proposed approach (see next section), we expect that the power distribution between two successive steps is not very different and so is the SNR. Therefore, the noise covariance matrix \mathbf{R}_{t+1} , which is inversely proportional to the SNR, is not significantly different from the \mathbf{R}_t at the previous time points. To exploit this correlation, could be reasonable to use the covariance matrix estimated by (26). However, (26) depends on the power received at time t , which is affected by the power allocation terms $\beta_k^{(t)}$ evaluated in the previous time step, hence directly using (26) to evaluate $\check{\mathbf{K}}_{t+1}$ would transfer the effect of the previous optimization to the next. Accordingly, we take:

$$\left\{ \check{\mathbf{R}}_t \right\}_{n,n} = \frac{\left[\beta_k^{(t)} \right]^2}{P_{\text{tx}}/K} \cdot \frac{\sigma^2(1+\alpha)}{\|\mathbf{y}_k\|^2/N_{\text{RX}}}, \quad (39)$$

for $n \in \mathcal{I}_k$. Note that $\check{\mathbf{R}}_t$ is an estimate of the noise covariance matrix when all RISs are assigned the same power P_{tx}/K , and as such it is independent of the prior power allocation strategy. In what follows, for notational convenience, we omit the dependence of all quantities involved on time $t+1$ and t unless explicitly required. Starting from (37) and considering only the terms depending on the optimization variable $\boldsymbol{\vartheta}$, the optimal parameters of the transmission configuration are obtained by solving the problem:

$$\begin{aligned} \min_{\boldsymbol{\vartheta}} \text{Tr} \left(\tilde{\mathbf{K}} \mathbb{E}_{\mathbf{p}} \{ \mathbf{R}(\mathbf{p}, \boldsymbol{\vartheta}) \} \tilde{\mathbf{K}}^T \right), \\ \text{s.t. } \boldsymbol{\vartheta} \in \mathcal{Q} \end{aligned}, \quad (40)$$

where $\mathbb{E}_{\mathbf{p}} \triangleq \mathbb{E}_{\mathbf{p}_{t+1|t}}$ is the expectation with respect to the position only, being the quantities only depending on \mathbf{p} .

The proof of the equivalence between (37) and (40) can be found in the supplementary material in Appendix B.

Let us denote by \mathbf{u}_n the n th column of $\tilde{\mathbf{K}}$. Thus, by introducing $\xi_k = \sigma^2(1+\alpha) \sum_{n \in \mathcal{I}_k} \|\mathbf{u}_n\|^2$, the problem can be further reformulated as

$$\begin{aligned} \min_{\boldsymbol{\vartheta}} \sum_{k=1}^K \xi_k \mathbb{E}_{\mathbf{p}} \{ (P_k(\mathbf{p}, \boldsymbol{\vartheta}_k))^{-1} \} \\ \text{s.t. } \boldsymbol{\vartheta} \in \mathcal{Q} \end{aligned}. \quad (41)$$

Let us now introduce $P_k^{(0)}(\mathbf{p}, \mathbf{c}_k)$ as the received power corresponding to unitary power distribution. Consequently, the actual received power is $P_k(\mathbf{p}, \boldsymbol{\vartheta}_k) = [\beta_k]^2 P_k^{(0)}(\mathbf{p}, \mathbf{c}_k)$ and we can recast problem (41) as

$$\begin{aligned} \min_{\boldsymbol{\vartheta}} \sum_{k=1}^K \xi_k \frac{1}{[\beta_k]^2} \mathbb{E}_{\mathbf{p}} \left\{ P_k^{(0)}(\mathbf{p}, \mathbf{c}_k)^{-1} \right\} \\ \text{s.t. } \boldsymbol{\vartheta} \in \mathcal{Q} \end{aligned}. \quad (42)$$

Since the k th RIS design concerns only the term $\mathbb{E}_{\mathbf{p}} \left\{ P_k^{(0)}(\mathbf{p}, \mathbf{c}_k)^{-1} \right\}$, the design criterion for the RISs becomes directly an SNR optimization criterion considering the possible UEs positions, i.e.

$$\begin{aligned} \min_{\mathbf{c}_k} \mathbb{E}_{\mathbf{p}} \left\{ P_k^{(0)}(\mathbf{p}, \mathbf{c}_k)^{-1} \right\} \\ \text{s.t. } |c_{k,p}| \leq 1, \forall p \in \mathcal{P} \end{aligned}. \quad (43)$$

Let us assume that problem (43) is solved and let us denote by \mathbf{c}_k^* and π_k , respectively, the optimal \mathbf{c}_k and the value of the objective function, i.e.,

$$\pi_k = \mathbb{E}_{\mathbf{p}} \left\{ P_k^{(0)}(\mathbf{p}, \mathbf{c}_k^*)^{-1} \right\}. \quad (44)$$

Hence, the precoder optimization problem can be written in the form of a power splitting problem among different RISs, i.e.,

$$\begin{aligned} \min_{\beta_k} \quad & \sum_{k=1}^K \gamma_k \frac{1}{\beta_k^2} \\ \text{s.t.} \quad & \sum_{k=1}^K [\beta_k]^2 \leq P_{\text{tx}}, \end{aligned} \quad (45)$$

where $\gamma_k = \xi_k \pi_k$.

VI. RIS AND PRECODER OPTIMIZATION FOR USER TRACKING: PROPOSED SOLUTIONS

A. RIS Optimization

Let us first focus on problem (43). From the assumption that each UE antenna receives the same power, the power of the signal coming from the k -th RIS can be evaluated as the power coming from the first UE antenna, i.e.:

$$P_k^{(0)}(\mathbf{p}, \mathbf{c}_k) = (\mathbf{v}_k^{(0)})^H \mathbf{G}_k^H \mathbf{C}_k^H \mathbf{b}_k^H(\mathbf{p}) \mathbf{b}_k(\mathbf{p}) \mathbf{C}_k \mathbf{G}_k \mathbf{v}_k^{(0)} \quad (46)$$

where $\mathbf{b}_k(\mathbf{p}) \in \mathbb{C}^{1 \times P}$ is the first row of $\mathbf{B}_k(\mathbf{p})$ corresponding to the first receiving antenna, and we recall that $\mathbf{C}_k = \text{diag}(\mathbf{c}_k)$ is the matrix containing the RIS coefficients vector. Without loss of generality, the index k is neglected from now on, and a formulation valid for every RIS is obtained. The goal of the RIS optimization in (43) is to find the beamforming vector \mathbf{c} such that the (statistical) average of the inverse of (46) over the uncertainty range of \mathbf{p} is minimized. Consequently, we can formulate (43) as

$$\begin{aligned} \min_{\mathbf{c}} \quad & \int P^{(0)}(\mathbf{p}, \mathbf{c})^{-1} f_{\mathbf{p}}(\mathbf{p}) d\mathbf{p} \\ \text{s.t.} \quad & |c_p|^2 \leq 1 \quad \forall p \in \mathcal{P}, \end{aligned} \quad (47)$$

where $f_{\mathbf{p}}(\mathbf{p})$ is the a-priori probability density function (pdf) of the position \mathbf{p} . In particular, from the EKF model, we have $f_{\mathbf{p}}(\mathbf{p}) = \mathcal{N}(\mathbf{p}; \mathbf{m}_{t+1|t}^{\{1:3\}}, \Sigma_{t+1|t}^{\{1:3,1:3\}})$.⁹ The problem (47) is non-convex and therefore, we propose below an iterative BCD algorithm to find a local optimum.

a) *BCD Algorithm*: For the sake of notation, we set $\mathbf{g} \triangleq \mathbf{G}\mathbf{v}^{(0)}$ and we consider the following equivalence

$$\mathbf{b}(\mathbf{p})\mathbf{C}\mathbf{g} = \mathbf{b}(\mathbf{p})\text{diag}(\mathbf{g})\mathbf{c} = \tilde{\mathbf{h}}(\mathbf{p})\mathbf{c}, \quad (48)$$

where $\tilde{\mathbf{h}}(\mathbf{p}) \triangleq \mathbf{b}(\mathbf{p})\text{diag}(\mathbf{g}) \in \mathbb{C}^{1 \times P}$. Accordingly, (46) simplifies as

$$P^{(0)}(\mathbf{p}, \mathbf{c}) = \mathbf{c}^H \tilde{\mathbf{h}}^H(\mathbf{p}) \tilde{\mathbf{h}}(\mathbf{p}) \mathbf{c}. \quad (49)$$

Let us introduce the following term:

$$\Sigma(\mathbf{p}, \mathbf{c}) = \frac{\delta}{P^{(0)}(\mathbf{p}, \mathbf{c}) + \delta}. \quad (50)$$

⁹The notations $\mathbf{m}_{t+1|t}^{\{1:3\}}$ and $\Sigma_{t+1|t}^{\{1:3,1:3\}}$ indicate respectively the first three elements of $\mathbf{m}_{t+1|t}$ and the first 3×3 matrix block of $\Sigma_{t+1|t}$.

When δ is small, we can recast problem in (47) as

$$\begin{aligned} \min_{\mathbf{c}} \quad & \int \Sigma(\mathbf{p}, \mathbf{c}) f_{\mathbf{p}}(\mathbf{p}) d\mathbf{p} \\ \text{s.t.} \quad & |c_p|^2 \leq 1, \quad \forall p \in \mathcal{P}. \end{aligned} \quad (51)$$

Then, we introduce

$$\Upsilon(\mathbf{p}, \mathbf{c}, w) = 1 + |w|^2 P^{(0)}(\mathbf{p}, \mathbf{c}) - 2\Re\{w \tilde{\mathbf{h}}(\mathbf{p})\mathbf{c}\} + \delta |w|^2, \quad (52)$$

where w is a complex parameter. It is straightforward to get the equivalence

$$\Sigma(\mathbf{p}, \mathbf{c}) = \min_w \Upsilon(\mathbf{p}, \mathbf{c}, w) = \Upsilon(\mathbf{p}, \mathbf{c}, w^*), \quad (53)$$

where

$$w^* = \frac{\mathbf{c}^H \tilde{\mathbf{h}}^H(\mathbf{p})}{P^{(0)}(\mathbf{p}, \mathbf{c}) + \delta}. \quad (54)$$

Accordingly, the problem in (47) can be reformulated as

$$\begin{aligned} \min_{\mathbf{c}} \quad & \int \min_w [\Upsilon(\mathbf{p}, \mathbf{c}, w)] f_{\mathbf{p}}(\mathbf{p}) d\mathbf{p} \\ \text{s.t.} \quad & |c_p|^2 \leq 1, \quad \forall p \in \mathcal{P}. \end{aligned} \quad (55)$$

Note that when δ tends to zero, $\Sigma(\mathbf{p}, \mathbf{c})$ in (53) also tends to zero for each \mathbf{c} and \mathbf{p} and the problem (55) cannot provide a meaningful solution. Therefore, δ must be chosen appropriately so that the problem (55) is not starved in the zero solution, and, at the same time, $\delta \ll P^{(0)}(\mathbf{p}, \mathbf{c})$ to ensure equivalence between (47) and (51). This aspect is explained in more detail below.

Although (55) is not convex, it is convex for the remaining variable if one of the two variables is fixed. As a result, a good local optimum can be obtained using the iterative BCD approach [49], where all variables involved are updated sequentially at each iteration. To illustrate this, we denote by $\mathbf{c}^{(q)}$ the value of \mathbf{c} after the q th iteration of BCD. From (54) we can then compute $w^{(q)}$ as follows

$$w^{(q)}(\mathbf{p}) = \frac{(\mathbf{c}^{(q)})^H \tilde{\mathbf{h}}^H(\mathbf{p})}{P^{(0)}(\mathbf{p}, \mathbf{c}^{(q)}) + \delta^{(q)}}, \quad (56)$$

where

$$\delta^{(q)} = \frac{\min_{\mathbf{p}} P^{(0)}(\mathbf{p}, \mathbf{c}^{(q)})}{M}, \quad (57)$$

with $M \gg 1$. The optimal choice of M depends on the trade-off between fast convergence (M must not be excessively high) and equivalence between (47) and (51) (M must be high). Finding an analytical approach to optimally deal with this trade-off is a very complex task. However, based on numerical considerations, we found that a value of $M = 100$ is a good compromise and, therefore, we set this value in the numerical results section. In (47) and (51) the problem of finding the optimal $\mathbf{c}^{(q+1)}$ for a given $w^{(q)}$ can be solved as follows. Let us first introduce the terms

$$\begin{aligned} \mathbf{A}^{(q)} &= \int |w^{(q)}(\mathbf{p})|^2 \tilde{\mathbf{h}}^H(\mathbf{p}) \tilde{\mathbf{h}}(\mathbf{p}) f_{\mathbf{p}}(\mathbf{p}) d\mathbf{p} \in \mathbb{C}^{P \times P} \\ \mathbf{s}^{(q)} &= \int w^{(q)}(\mathbf{p}) \tilde{\mathbf{h}}(\mathbf{p}) f_{\mathbf{p}}(\mathbf{p}) d\mathbf{p} \in \mathbb{C}^{1 \times P} \in \mathbb{C}^{1 \times P} \end{aligned} \quad (58)$$

which can be computed by numerical integration. Therefore, the optimal \mathbf{c} for a given $w^{(q)}(\mathbf{p})$ can be found from

$$\begin{aligned} \min_{\mathbf{c}} \quad & \mathbf{c}^H \mathbf{A}^{(q)} \mathbf{c} - 2\Re\{\mathbf{s}^{(q)} \mathbf{c}\} \\ \text{s.t.} \quad & |c_p|^2 \leq 1, \forall p \in \mathcal{P}. \end{aligned} \quad (59)$$

This is a convex problem that can be solved using traditional numerical approaches whose solution will be denoted as OPT in the sequel. However, the inclusion of a large number of inequality constraints makes the problem computationally difficult when P is high. An iterative strategy based on alternating optimization (AO), where optimization is performed at each step for a single element c_p while the others remain fixed, is one way to simplify the problem. The AO approach will be referred to as OPT-AO. We will show in the results that OPT-AO achieves performance very close to that of OPT while noticeably reducing computational complexity. To elaborate, consider the following problem

$$\begin{aligned} \min_{c_p} \quad & \mathbf{c}^H \mathbf{A}^{(q)} \mathbf{c} - 2\Re\{\mathbf{s}^{(q)} \mathbf{c}\} \\ \text{s.t.} \quad & |c_p|^2 \leq 1, \end{aligned} \quad (60)$$

where the difference with respect to (59) is that the minimum is searched for each c_p independently. The solution to this problem can be found in closed form by enforcing the Karush Kuhn Tucker (KKT) optimality conditions. In particular, the Lagrangian function, with the multiplier λ_p , is

$$L(c_p, \lambda_p) = \mathbf{c}^H \mathbf{A}^{(q)} \mathbf{c} - 2\Re\{\mathbf{s}^{(q)} \mathbf{c}\} + \lambda_p (|c_p|^2 - 1). \quad (61)$$

Considering the KKT conditions we have

$$\nabla_{c_p} L(c_p, \lambda_p) = 2\mathbf{a}_p^{(q)} \mathbf{c} - 2\left(s_p^{(q)}\right)^* + 2\lambda_p c_p = 0 \quad (62)$$

$$\lambda_p \geq 0 \quad (63)$$

$$\lambda_p (|c_p|^2 - 1) = 0, \quad (64)$$

where $\mathbf{a}_p^{(q)} \in \mathbb{C}^{1 \times P}$ is the p th row of $\mathbf{A}^{(q)}$, $s_p^{(q)}$ is the p th element of $\mathbf{s}^{(q)}$ and the second condition is the complementary slackness condition. Denote by $V_p = \sum_{l \neq p} a_{p,l}^{(q)} c_l$, $A_p = a_{p,p}^{(q)}$, and $Y_p = (s_p^{(q)})^* - V_p$, where $a_{p,l}^{(q)}$ is the l th element of $\mathbf{a}_p^{(q)}$, it is then easy to derive from (62)

$$\begin{aligned} c_p &= Y_p / A_p, \lambda_p = 0 & \text{if } |Y_p| < |A_p| \\ c_p &= Y_p / |Y_p|, \lambda_p = |Y_p| - A_p & \text{if } |Y_p| \geq |A_p|. \end{aligned} \quad (65)$$

B. Precoder Optimization

The precoder optimization problem presented in (45) can be easily solved by resorting to the KKT constraints. Writing the Lagrangian function as

$$L(\beta_k, \lambda) = \sum_{k=1}^K \frac{\gamma_k}{\beta_k^2} + \lambda \left(\sum_{k=1}^K \beta_k^2 - P_{\text{tx}} \right), \quad (66)$$

the KKT conditions can be derived as

$$\nabla_{\beta_k} L(\beta_k, \lambda) = -2 \frac{\gamma_k}{(\beta_k^*)^3} + 2\lambda^* \beta_k^* = 0 \quad (67)$$

$$\sum_{k=1}^K (\beta_k^*)^2 - P_{\text{tx}} \leq 0 \quad (68)$$

$$\lambda^* \geq 0 \quad (69)$$

$$\lambda^* \left(\sum_{k=1}^K (\beta_k^*)^2 - P_{\text{tx}} \right) = 0. \quad (70)$$

The existence conditions of the given equations are summarized as $\beta_k^* \neq 0$ and $\lambda^* \neq 0$, and thus, it is easy to derive the optimal solution as

$$\lambda^* = \frac{\left(\sum_{k=1}^K \sqrt{\gamma_k} \right)^2}{P_{\text{tx}}^2}, \quad (\beta_k^*)^2 = \frac{\sqrt{\gamma_k} P_{\text{tx}}}{\sum_{k=1}^K \sqrt{\gamma_k}}. \quad (71)$$

The proposed power allocation strategy at each time t is not simply a matter of optimizing the SNR of each connection but a much broader problem, similar to water-filling where most of the power is distributed in favor of the channels with the highest SNR to maximize the achievable communication rate. However, in our case, the power weights depend, among other factors, on the Kalman gains defined in (38), which in turn depend on the Jacobian matrices evaluated considering the near-field propagation model between the RIS and the UE. Therefore, the near-field model is exploited at each stage of the proposed strategy.

C. Two-Timescale Optimization

As discussed in Section II, RIS and precoding optimization are performed on two different time scales. As for the precoding, the time scale corresponds to the interval between two consecutive pilot signal transmissions and may be on the order of a few milliseconds, e.g., on the same time scale as channel estimation in communications. This interval corresponds to the time between two successive location updates of the EKF algorithm and will be denoted by dt in the following. Conversely, the time scale of the RIS update, denoted by T_O , can be expected to be on the order of seconds, i.e., orders of magnitude higher. We denote with $N_r = T_O/dt$ the (integer) number of steps between two successive RIS optimizations. Thus, if the previous RIS optimization is performed at time t , in order to obtain the new optimization at time $t + N_r$ according to the approach presented in Section VI-A, the a-priori pdf $f_{\mathbf{p}}(\mathbf{p})$ must be defined to account for the N_r transitions of the EKF. More precisely, we have

$$\mathbf{m}_{t+q+1|t} = \mathbf{T} \mathbf{m}_{t+q|t}, \quad \Sigma_{t+q+1|t} = \mathbf{T} \Sigma_{t+q|t} \mathbf{T}^T + \mathbf{P}, \quad (72)$$

for $q = 1, \dots, N_r$. The pdf of the position \mathbf{p} at time $t + q$ is given by $f_{\mathbf{p}}^{(q)}(\mathbf{p}) = \mathcal{N}(\mathbf{m}_{t+q+1|t}, \Sigma_{t+q+1|t})$ and

$$f_{\mathbf{p}}(\mathbf{p}) = \frac{1}{N_r} \sum_{q=1}^{N_r} f_{\mathbf{p}}^{(q)}(\mathbf{p}). \quad (73)$$

The terms in (58) are then evaluated using Monte Carlo numerical integration by drawing samples according to (73). The algorithms for RIS and precoder optimization are sketched in Algorithm 2, where N_{BCD} indicates the number of iterations of the BCD, and Algorithm 3. Fig. 2 schematically represents the whole procedure entailing joint RIS and precoder optimization with UE tracking.

Algorithm 2: RIS Optimization with BCD Approach

Uncertainty area construction;
for $q = 1, \dots, N_r$ **do**
 | Compute $f_p^{(q)}(\mathbf{p})$ according to (72)–(73);
end
 $f_p(\mathbf{p}) = \frac{1}{N_r} \sum_{q=1}^{N_r} f_p^{(q)}(\mathbf{p})$;
RIS Parameter Update;
Initialize $\mathbf{c}^* = \mathbf{c}_k^{(t)}$;
for $q = 1, \dots, N_{BCD}$ **do**
 | Initialize the iterative solution: $\mathbf{c}^{(q)} = \mathbf{c}^*$;
 | Update $w^{(q)}$, $\mathbf{A}^{(q)}$ and $\mathbf{s}^{(q)}$ according to (56)–(58);
 for $p = 1, \dots, P$ **do**
 | Solve problem (60) for c_p as in (65);
 end
end
 $\mathbf{c}_k^{(t+1)} = \mathbf{c}^*$

VII. RESULTS

This simulation study aims to evaluate the validity of the optimized RIS-based UE tracking approach in a typical indoor scenario according to the following approaches:

- The optimization approach described in Section VI-A with uniform power allocation for the different RISs¹⁰, i.e., $\beta_k^2 = P_{\text{tx}}/K$, referred as OPT, and its approximation obtained using the AO method (Algorithm 2), referred as OPT-AO.
- The optimization approach described in Section VI-A with optimal power allocation, denoted by βOPT , and its AO version (Algorithm 2) denoted as $\beta\text{OPT-AO}$. In both cases, power allocation (BS precoding) is performed according to Algorithm 3.
- The FOCUS and βFOCUS approaches, in which the RIS design is performed to maximize the reflected power in the direction of the position estimate, as proposed in [30], while the power is allocated uniformly (FOCUS) or according to the Algorithm 3 (βFOCUS).
- The ROPT approach, in which the RIS design is performed with the goal of maximizing the average communication rate when a-priori statistical knowledge about the UE location is available and given by $f_p(\mathbf{p})$. This approach has been proposed in [20], and the power is uniformly allocated. We use this algorithm to investigate the loss of tracking performance occurring when RISs and precoders are not optimized for localization purposes and to study the trade-off that occurs between rate and position error when communication or localization objective functions are considered.

A. Complexity Analysis

The two-time scale optimization approach allows us to consider the complexity problem as divided into two parts. During the shorter time scale operations, i.e., the location update time

¹⁰Uniform power allocation means that the joint RIS-BS precoder optimization results in BD precoding with uniform power and RIS optimization.

Algorithm 3: Optimization for Target Tracking

for $k = 1, \dots, K$ **do**
 if $N_r | t$ **then**
 | Optimize the RIS computing the new $\mathbf{c}_k^{(t+1)}$;
 else
 | $\mathbf{c}_k^{(t+1)} = \mathbf{c}_k^{(t)}$
 end
 Evaluate $\tilde{\mathbf{K}}$ (see eq. (38)), \mathbf{u}_n and compute \mathcal{I}_k ;
 $\xi_k = \sigma_k^2 \sum_{n \in \mathcal{I}_k} \|\mathbf{u}_n\|^2$;
 $\mathbf{c}_k^* = \mathbf{c}_k^{(t+1)}$;
 Compute π_k according to (44);
 $\gamma_k = \xi_k \pi_k$;
 $[\beta_k^{(t+1)}]^2 = \frac{\sqrt{\gamma_k} P_{\text{tx}}}{\sum_{k=1}^K \sqrt{\gamma_k}}$;
end

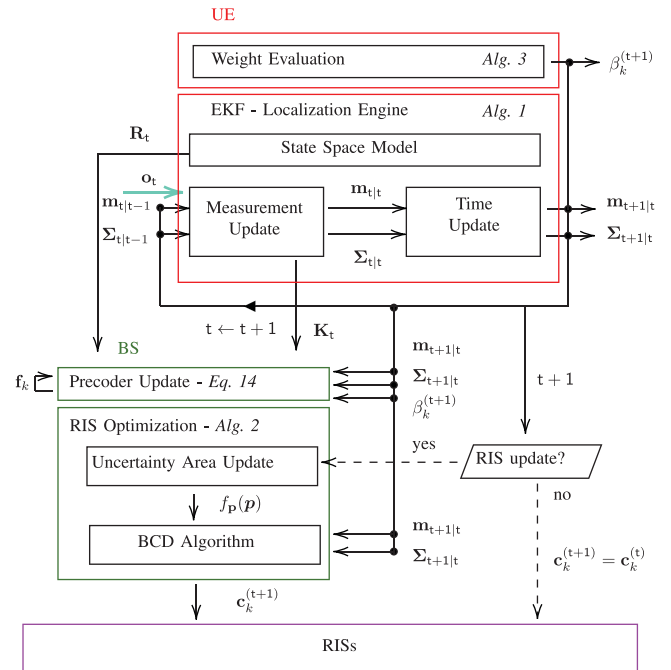


Fig. 2. Interconnections between localization, RIS optimization, and BS precoding algorithms.

of dt seconds, the complexity of all algorithms is the same and is equal to the complexity of the standard EKF for tracking. In this phase, the complexity is dominated by the computation of the inverse of the covariance matrix of the innovation, which is $\mathcal{O}(K^3 N_{\text{RX}}^3)$, where K is the number of RIS and N_{RX} is the number of receiving antennas. On the other hand, the RIS design is clearly the bottleneck in terms of computational complexity since it involves solving a high-dimensional optimization problem whose dimension depends on a large number of RIS elements. In this respect, the considered approach OPT-AO allows a significant complexity reduction compared to traditional RIS optimization schemes denoted as ROPT. More precisely, the complexity of the proposed algorithm OPT-AO is $\mathcal{O}(P)$, i.e., it is linear with the number of RIS elements (see Eq. (65)), while the complexity of the rate optimization scheme proposed in [20] is $\mathcal{O}(P^3)$. Accordingly, the complexity of

TABLE I
SYSTEM PARAMETERS FOR THE SIMULATION CONFIGURATION

PARAMETER	VALUE
Carrier frequency	$f_c = 28$ GHz
Subcarrier Bandwidth	$B_c = 120$ kHz
Transmit power	$P_{tx} = 23$ dBm
Noise power density	$NPD = -174$ dB/Hz
Noise Figure	$NF = 7$ dB
Rice Factor	$\kappa_b = 5$
Empirical parameter for (26) and (39)	$\alpha = 0.5$

OPT-AO is comparable to that of the simple FOCUS approach, which is also linear with P . However, it is worth noting that RIS optimization in the proposed scheme is performed on a long time scale (once every T_O second), and therefore the complexity issues are significantly mitigated.

B. Parameter Settings

We refer to the 3GPP specifications for 5G localization in indoor open office (IOO) scenarios and the corresponding results reported in [50]. Some of the system parameters are reported in Table I with some of them adjusted to match the narrow-band RIS-based near-field localization scenario considered in this work. Specifically, in the proposed scenario, localization is performed over a single 120kHz subcarrier band with a correspondent pilot symbol time $T_s = 8.3\mu s$. The transmitted pilot signal consists of $L = 100$ symbols, corresponding to a time of $\tau = 100 \cdot T_s = 0.83ms$. To reduce the localization overhead, the pilot signal is transmitted periodically every $dt \gg \tau$. Localization and power allocation are thus performed every dt seconds, while the RIS optimization procedure is performed every $T_O = N_r \cdot dt$ seconds. We assume that the total available power is uniformly distributed over the entire spectrum, i.e., a power $P_{tx} = 0.06mW$ for the transmission of the pilot signal is allocated. We also consider a simple Rice channel model for the RIS-UE channel (see (9)), i.e., we assume that the LOS component is always present, and we consider an uncorrelated NLOS component.¹¹

The system geometry is sketched in Fig. 3. The BS is at a fixed position, namely at $\mathbf{p}_{TX} = [30, 15, 2]$ m, and it has a uniform rectangular array (URA) with 8×2 antennas in the YZ -plane. The UE changes positions through time according with (16)¹² and it is equipped with a uniform linear array (ULA) of four antennas, lying horizontally along the Y -axis and with a fixed and known orientation. For the motion of the UE, to emulate a movement pattern compatible with a typical random pedestrian motion model, we set $\sigma_{a,x}^2 = \sigma_{a,y}^2 = 0.5 \text{ m}^2/\text{s}^3$, $\sigma_{a,z}^2 = 0 \text{ m}^2/\text{s}^3$. In all simulations, it is assumed that the initial state of the node (i.e., its position and velocity) is known, i.e., $\mathbf{m}_0 = \mathbf{s}_0$ and $\Sigma_0 = \mathbf{P}$. There are three RISs in the environment located at $[0, 15, 3]$ m, $[5, 0, 3]$ m, $[10, 30, 3]$ m, if not otherwise indicated. They consist of a URA of 80×5 elements lying

¹¹The first assumption is reasonable because in the near-field region, the distance between RISs and UE is small and the LOS probability is close to 1 [51]. As for the second assumption, uncorrelated scattering is a reasonable model without well-established channel models to characterize the RIS-UE channel.

¹²The z coordinate is kept fixed at 1 m.

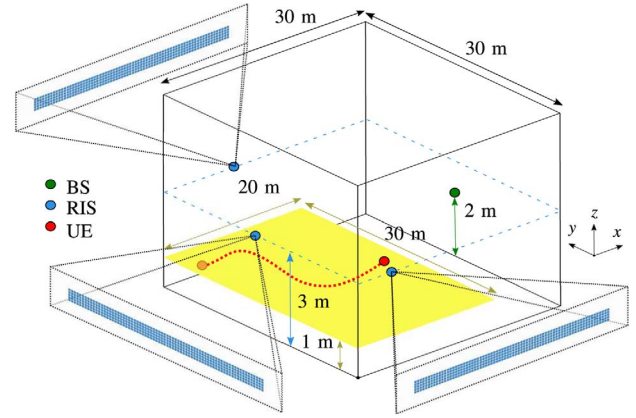


Fig. 3. Working scenario with an example of UE trajectory.

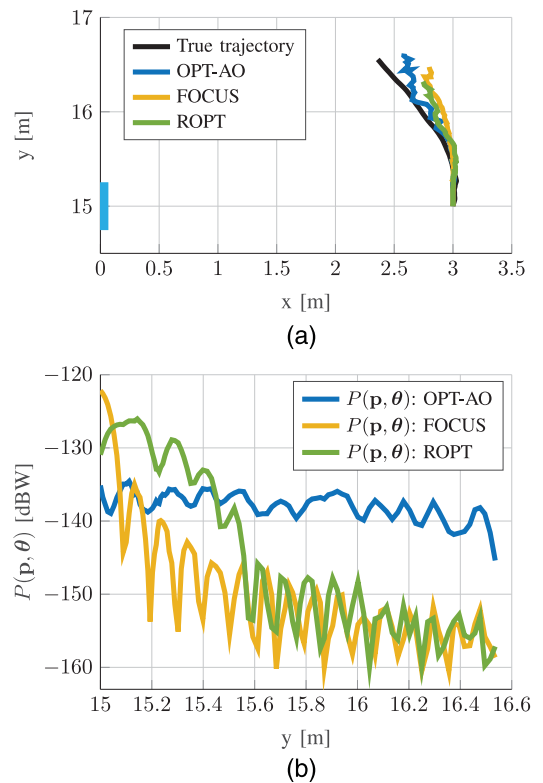


Fig. 4. Comparison between OPT-AO, FOCUS, and ROPT for a 3-second trajectory in terms of: (a) estimated trajectory, (b) received power.

on the YZ -plane, i.e., they are mainly used in the horizontal direction as long strips. In this way, the maximum dimension of the RIS is nearly 40cm and the radiating near-field extends over about 32m.

C. Tracking Scenario

In Fig. 4(a), we consider a simplified scenario to present a graphical representation of possible estimated trajectories and to show the corresponding RIS power distributions in Figs. 4(b) and 5. In this scenario, there is only the RIS at position $(0, 15)m$ and the terminal travels a 3-second trajectory starting at point $(3, 15)m$, with an initial speed of $1m/s$ in the y

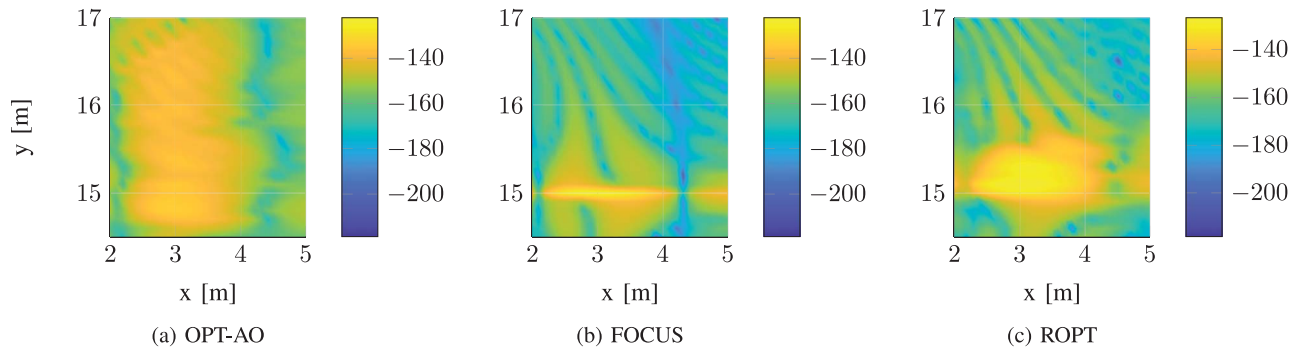


Fig. 5. Distribution of reflected RIS power in the scenario of Fig. 4 for the OPT-AO, FOCUS, and ROPT cases.

direction.¹³ The figure shows the actual node trajectory and the trajectories obtained considering RIS optimization performed through the approaches OPT-AO, FOCUS, and ROPT. The RIS is only optimized once at time 0, while the location update is performed every $dt = 0.03$ seconds, i.e., we have 100 location updates. For this short trajectory, having a single RIS is sufficient to achieve good localization performance, especially when the OPT-AO scheme is considered. In contrast, the ROPT and FOCUS optimization leads to larger estimation errors.

The reason for this behavior can be explained by analyzing Fig. 4(b), where the received power expressed in dBW is plotted as a function of the y coordinate for the three systems under consideration. It is obvious that the FOCUS scheme maximizes the energy at the estimated point at time 0 (i.e. when the UE is at $y = 15$ m), but it leads to a huge power penalty as long as the terminal moves from its starting point. On the other hand, the OPT-AO scheme allows the power to be balanced over the entire interval, while the ROPT method concentrates the energy on the central part of the uncertainty range and spares the outer edges. Although this may be optimal for obtaining the maximum average rate, as shown below, it is inconvenient for localization.

In Fig. 5, we show the distribution of reflected RIS power in the operational scenario of Fig. 4 for the cases OPT-AO, FOCUS, and ROPT, respectively. The power value at each point on the map is shown with different colors, with the color bar on the right indicating the power levels in dBW. It can be seen that the OPT-AO approach, Fig. 5(a), provides a nearly uniform distribution of the received power over the uncertainty range, the FOCUS approach, Fig. 5(b), concentrates the power in a small area around the estimated starting point (3, 15)m, while the ROPT approach, Fig. 5(c), provides uniform distribution in a limited area with respect to OPT-AO.

D. Simulation Results

In the following, we report a comprehensive comparative simulation study considering the operating environment of Fig. 3 with three RISs. The UE moves in a part of space with dimension $20\text{m} \times 30\text{m}$ denoted as the range of motion (RM), corresponding to the yellow area in Fig. 3. Note that in the considered space, we are always in the near-field region for

¹³Since we are considering a single RIS, all power is allocated to that RIS and power allocation is not effective, i.e., β OPT is equal to OPT.

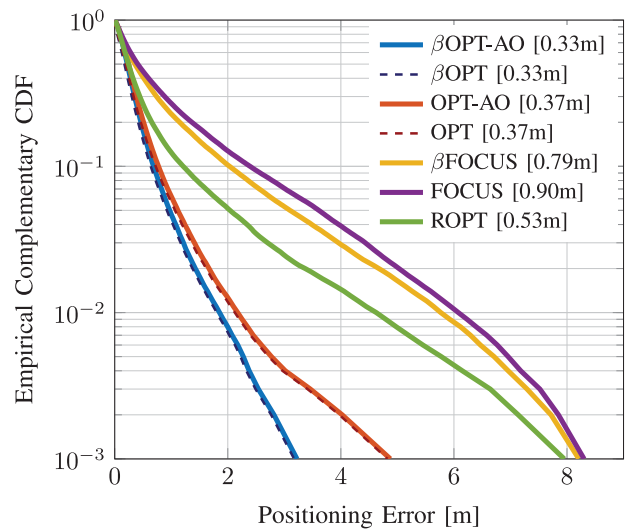


Fig. 6. Empirical complementary CDF of the localization error for different optimization approaches. In brackets there are the mean values of the localization errors.

all considered RISs. The UE is initially placed randomly and moves along a 12-second trajectory according to the motion model considered in this work. Statistics are collected in 1000 different simulations.

Fig. 6 shows the empirical complementary cumulative distribution function (CDF)¹⁴ of the localization error, indicating the probability (rate) that the localization error is above a threshold, for the cases FOCUS, β FOCUS, OPT, β OPT, OPT-AO, β OPT-AO, and ROPT. The results are here obtained by considering a Rice factor $\kappa_b = 5$, $dt = 0.03\text{s}$, and $N_r = 100$, i.e., $T_O = 3\text{s}$. The choice of this RIS update time is closely related to the motion model employed for the UE. Indeed, by considering a typical random pedestrian motion model, as in (16), (18), an update of $T_O = 3\text{s}$ entails a UE movement of few meters that is compatible with the sub-meter localization accuracy. In the following, a further comparison for different T_O values has been provided as well.

In Fig. 6, first we show that OPT-AO and β OPT-AO achieve the same performance as OPT and β OPT, confirming the validity of the AO approximation proposed in Section VI-A.

¹⁴The reason for reporting 1-CDF is to highlight the differences at low positioning errors and to avoid possible curve overlaps.

TABLE II
RESULTS FOR THE CASE β OPT-AO FOR DIFFERENT VALUES OF THE RICE FACTOR κ_b IN TERMS OF THE LOCALIZATION ERROR EXPRESSED IN METERS

κ_b	Mean value	0.9 performance	0.99 performance
$\kappa_b = 2$	0.38	0.78	2.17
$\kappa_b = 5$	0.33	0.69	1.92
$\kappa_b = 100$	0.29	0.59	1.58

Moreover, the proposed approach OPT-AO significantly outperforms both FOCUS and ROPT, which confirms the validity of the proposed RIS optimization for the localization procedure. Considering, in particular, 90% CDF (i.e., 10% 1-CDF), the results show that OPT-AO and β OPT-AO achieve an error below one meter. Regarding the mean localization errors (indicated in parentheses), we note that β OPT-AO has an average value of 33 cm, which increases to 53 and 79 cm for ROPT and β FOCUS, respectively. Finally, optimizing β can lead to some improvement in localization error performance, which is particularly evident for the case OPT-AO at high CDF values (i.e., at low 1-CDF).

In Table II, we provide the results for the case β OPT-AO for different values of the Rice factor κ_b . It can be seen that for the case shown in Fig. 6 ($\kappa_b = 5$), a slight performance degradation is observed compared to the LOS case ($\kappa_b = 100$). When the LOS component is further reduced, e.g., for $\kappa_b = 2$, the degradation increases as expected, although this does not affect the validity of the proposed approach.

Within our study we also provide some results on communication rates and localization errors, which depend on how the objective function for the RIS optimization problem is defined. In our work, the RIS optimization problem is formulated such that the UE tracking performance is maximized (e.g., solved by the β OPT-AO algorithm). Therefore, we expect the results to be better in terms of positioning accuracy compared to scenarios where RISs had been optimized in favor of communication and vice versa. To emphasize this point, we refer to Fig. 7 in which the mean localization error (a), the average achievable rate (b), and their trade-off (c) for the algorithms β FOCUS, β OPT-AO and ROPT are shown for different T_O values and for $dt = 0.03$ s. As expected, the localization error decreases with the decrease of T_O for all methods considered, while β OPT-AO clearly outperforms the other methods in all cases. Regarding the communication part, we do not consider additional pilots that would be necessary for the CSI estimation and the corresponding precoder optimization, as these aspects are beyond the scope of this work. Instead, we consider Shannon's standard formula to obtain an estimate of the achievable rate. In other words it is defined as the capacity in bits/s/Hz of the channel matrix $\mathbf{H}_{eq} = \sum_{k=1}^K \mathbf{B}_k \mathbf{C}_k \mathbf{G}_k$ with noise variance σ^2 , which can be determined by SVD and waterfilling.

Interestingly, it can be observed that, while the β OPT-AO approach prevails in terms of localization error, is the worst in terms of mean achievable rate. On the other hand, as expected, ROPT achieves the highest mean rate, given its specific design for communication purposes. A more detailed consideration can be made comparing the algorithms β OPT-AO and ROPT and considering the case $T_O = 3$ s, which shows that the

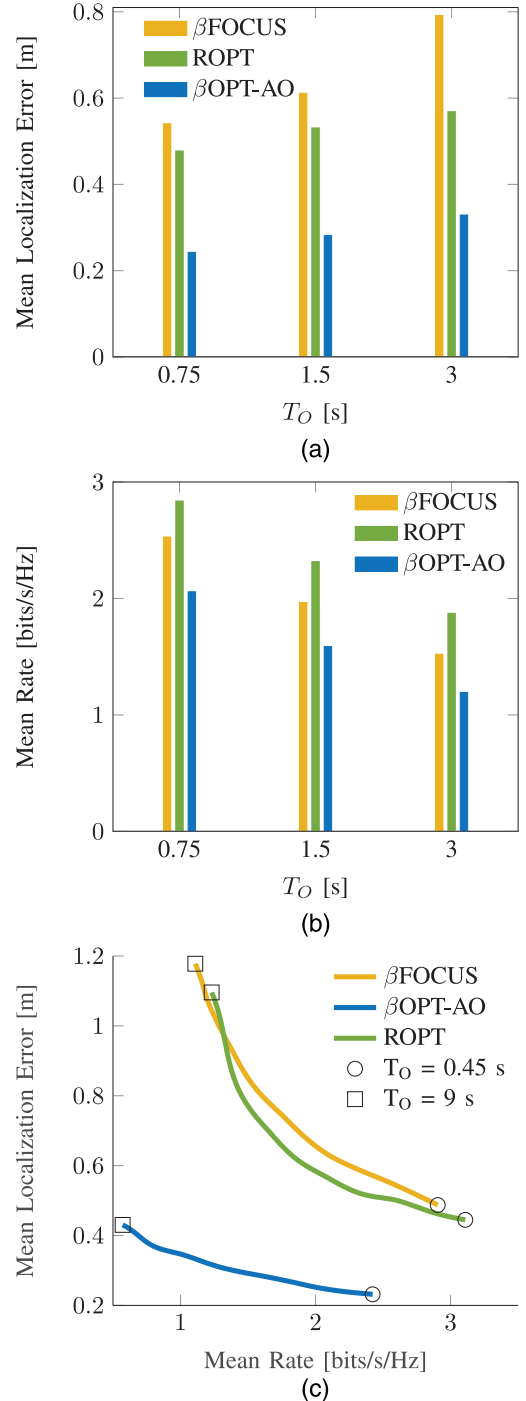


Fig. 7. Mean localization error (a) and mean rate (b) for β FOCUS, β OPT-AO, and ROPT algorithms computed for different T_O values and $dt = 0.03$ seconds. (c) Trade-off between mean localization error and mean rate computed for different values of T_O , sampled between 0.45 and 9 seconds.

proposed method β OPT-AO achieves a rate almost 35% lower than that of ROPT. Conversely, β OPT-AO achieves a 42% lower positioning error compared to ROPT. This trade-off between localization and communication is consistent across all the analyzed cases with different T_O and dt values. This is a non-obvious result since it is generally assumed that the best RIS optimization strategy is always to maximize the power in the direction where the node is (or should be) located.

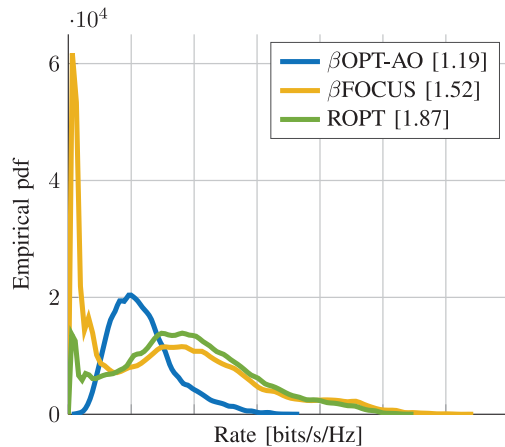


Fig. 8. Empirical pdf of the achievable average rate for β FOCUS, β OPT-AO, and ROPT.

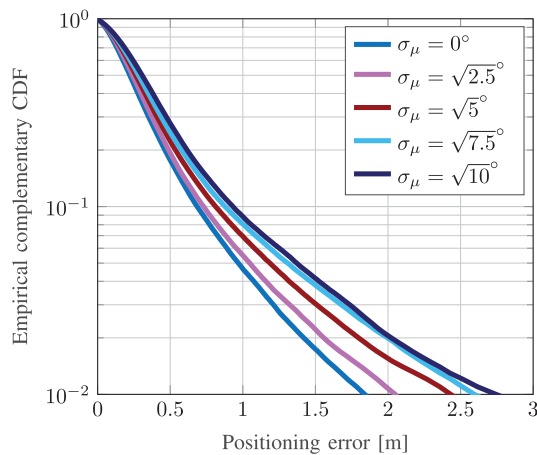


Fig. 9. Empirical complementary CDF of the positioning error for different orientation errors $\epsilon_\mu \sim \mathcal{N}(0, \sigma_\mu^2)$ with $\epsilon_\mu = \mu - \hat{\mu}$ being the orientation error computed as the difference of the true orientation angle (μ) and its estimate ($\hat{\mu}$), and with σ_μ being the standard deviation of the orientation estimator in degrees.

Furthermore, from Fig. 7(c), it can be seen that the proposed method β OPT-AO has an advantage over the other algorithms because, for the same T_O , the mean localization error for β OPT-AO is significantly smaller compared to the other cases, with only a slight decrease in rate.

In Fig. 8, we give the empirical pdf of the achievable rate for β FOCUS, β OPT-AO, and ROPT approaches. It can be seen that the β FOCUS and ROPT, although better than β OPT-AO in terms of mean rate, suffer from high probabilities of zero or quasi-zero rate, while β OPT-AO avoids such unpleasant situations and ensures a more consistent rate distribution.

In Fig. 9 we report the complementary empirical CDF of the positioning error for various orientation errors. This analysis aims to evaluate the robustness of the proposed β OPT-AO method in the presence of residual estimation errors when inferring the UE orientation from inertial devices, such as IMU [52], [53]. To assess this, we performed simulations in which the orientation of the UE is affected by an i.i.d. unbiased Gaussian error with a standard deviation ranging between $\sigma_\mu = 1^\circ$ and $\sigma_\mu = \sqrt{10}^\circ$. The result is promising as it shows that, in all cases, the localization error remains below 1 m for 90% of the time.

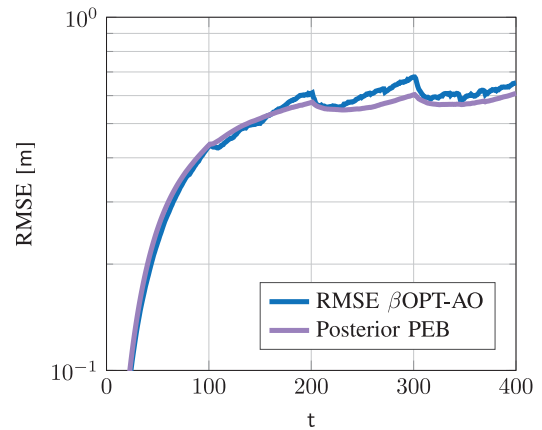


Fig. 10. Logarithmic representation of the posterior PEB vs RMSE for the β OPT-AO algorithm.

Finally, in Fig. 10 we show the root mean square error (RMSE) performance of our proposed algorithm (β OPT-AO) compared with the PEB [54]. The results exhibit a wavelike pattern with peaks aligned with the RIS optimization instants (one every 100 iterations) and a perfect match between the bound and the algorithm performance. The figure also highlights a transition period (of almost 150 iterations) during which the error increases, since we assumed zero error at the initial time.

VIII. CONCLUSIONS

In this paper, we have proposed a novel framework to jointly design the reflection coefficients of multiple RISs and the precoding strategy of a single BS, with two different time scales, to optimize the tracking of a single multi-antenna UE and to keep the overall system complexity affordable. The optimal derived RIS and precoding optimization approach has been compared with traditional focusing and rate maximization strategies, showing that RIS optimization for communication purposes is suboptimal when applied to tracking tasks. Numerical results have shown the potential of achieving highly accurate positioning in typical indoor environments only using a single BS and few RISs operating at millimeter waves. These findings align with the trends and requirements foreseen for the next 6G networks. Simulation results have revealed that having multiple and larger RISs can lead to a significant increase of the tracking performance provided that are properly jointly optimized.

REFERENCES

- [1] C. De Lima et al., "Convergent communication, sensing and localization in 6G systems: An overview of technologies, opportunities and challenges," *IEEE Access*, vol. 9, pp. 26902–26925, Jan. 2021.
- [2] Z. Wang et al., "Location awareness in beyond 5G networks via reconfigurable intelligent surfaces," *IEEE J. Sel. Areas Commun.*, vol. 40, no. 7, pp. 2011–2025, Jul. 2022.
- [3] K. Witrals et al., "High-accuracy localization for assisted living: 5G systems will turn multipath channels from foe to friend," *IEEE Signal Process. Mag.*, vol. 33, no. 2, pp. 59–70, Mar. 2016.
- [4] J. He et al., "Beyond 5G RIS mmWave systems: Where communication and localization meet," *IEEE Access*, vol. 10, pp. 68075–68084, Jun. 2022.
- [5] M. D. Renzo et al., "Smart radio environments empowered by reconfigurable AI meta-surfaces: An idea whose time has come," *EURASIP J. Wireless Commun. Netw.*, vol. 2019, no. 1, pp. 1–20, 2019.

- [6] E. Basar et al., "Wireless communications through reconfigurable intelligent surfaces," *IEEE Access*, vol. 7, pp. 116753–116773, Aug. 2019.
- [7] G. C. Alexandropoulos, N. Shlezinger, and P. del Hougne, "Reconfigurable intelligent surfaces for rich scattering wireless communications: Recent experiments, challenges, and opportunities," *IEEE Commun. Mag.*, vol. 59, no. 6, pp. 28–34, Jun. 2021.
- [8] R. Flamini et al., "Towards a heterogeneous smart electromagnetic environment for millimeter-wave communications: An industrial viewpoint," *IEEE Trans. Antennas Propag.*, vol. 70, no. 10, pp. 8898–8910, Oct. 2022.
- [9] H. Zhang et al., "Beam focusing for near-field multiuser MIMO communications," *IEEE Trans. Wireless Commun.*, vol. 21, no. 9, pp. 7476–7490, Sep. 2022.
- [10] H. Wymeersch et al., "Radio localization and mapping with reconfigurable intelligent surfaces: Challenges, opportunities, and research directions," *IEEE Veh. Technol. Mag.*, vol. 15, no. 4, pp. 52–61, Dec. 2020.
- [11] A. Elzanaty et al., "Reconfigurable intelligent surfaces for localization: Position and orientation error bounds," *IEEE Trans. Signal Process.*, vol. 69, pp. 5386–5402, 2021.
- [12] H. Zhang et al., "MetaLocalization: Reconfigurable intelligent surface aided multi-user wireless indoor localization," *IEEE Trans. Wireless Commun.*, vol. 20, no. 12, pp. 7743–7757, Dec. 2021.
- [13] D. Dardari et al., "LOS/NLOS near-field localization with a large reconfigurable intelligent surface," *IEEE Trans. Wireless Commun.*, vol. 21, no. 6, pp. 4282–4294, Jun. 2022.
- [14] F. Guidi and D. Dardari, "Radio positioning with EM processing of the spherical wavefront," *IEEE Trans. Wireless Commun.*, vol. 20, no. 6, pp. 3571–3586, Jun. 2021.
- [15] H. Wymeersch and G. Seco-Granados, "Radio localization and sensing—Part I: Fundamentals," *IEEE Commun. Lett.*, vol. 26, no. 12, pp. 2816–2820, Dec. 2022.
- [16] H. Chen et al., "A tutorial on terahertz-band localization for 6G communication systems," *IEEE Commun. Surveys Tuts.*, vol. 24, no. 3, pp. 1780–1815, thirdquarter 2022.
- [17] E. Björnson et al., "Reconfigurable intelligent surfaces: A signal processing perspective with wireless applications," *IEEE Signal Process. Mag.*, vol. 39, no. 2, pp. 135–158, Mar. 2022.
- [18] H. Zhang et al., "Towards ubiquitous positioning by leveraging reconfigurable intelligent surface," *IEEE Commun. Lett.*, vol. 25, no. 1, pp. 284–288, Jan. 2021.
- [19] C. L. Nguyen et al., "Wireless fingerprinting localization in smart environments using reconfigurable intelligent surfaces," *IEEE Access*, vol. 9, pp. 135526–135541, Sep. 2021.
- [20] A. Abrardo, D. Dardari, and M. Di Renzo, "Intelligent reflecting surfaces: Sum-rate optimization based on statistical position information," *IEEE Trans. Commun.*, vol. 69, no. 10, pp. 7121–7136, Oct. 2021.
- [21] W. Zhou et al., "Joint precoder, reflection coefficients, and equalizer design for IRS-assisted MIMO systems," *IEEE Trans. Commun.*, vol. 70, no. 6, pp. 4146–4161, Jun. 2022.
- [22] J. Dai et al., "Statistical CSI-based transmission design for reconfigurable intelligent surface-aided massive MIMO systems with hardware impairments," *IEEE Wireless Commun. Lett.*, vol. 11, no. 1, pp. 38–42, Jan. 2022.
- [23] B. Denis and H. Wymeersch, "Method for optimizing user equipment wireless localization using reconfigurable intelligent surfaces, related device and computer program," U.S. Patent Appl. 17/337 593, Dec. 2021.
- [24] M. Rahal et al., "Constrained RIS phase profile optimization and time sharing for near-field localization," in *Proc. IEEE 95th Veh. Technol. Conf. (VTC)*, Spring 2022, pp. 1–6.
- [25] P. Gao, L. Lian, and J. Yu, "Wireless area positioning in RIS-assisted mmWave systems: Joint passive and active beamforming design," *IEEE Signal Process. Lett.*, vol. 29, pp. 1372–1376, Jun. 2022.
- [26] Z. Feng et al., "Power optimization for target localization with reconfigurable intelligent surfaces," *Signal Process.*, vol. 189, Dec. 2021, Art. no. 108252.
- [27] F. Jiang et al., "Optimization of RIS-aided integrated localization and communication," 2022, *arXiv:2209.02828*.
- [28] S. Palmucci et al., "Reconfigurable intelligent surfaces: A joint localization and communication perspective," in *Proc. IEEE 95th Veh. Technol. Conf. (VTC)*, Piscataway, NJ, USA: IEEE, Spring 2022, pp. 1–5.
- [29] J. He et al., "Adaptive beamforming design for mmWave RIS-aided joint localization and communication," in *Proc. IEEE Wireless Commun. Netw. Conf. Workshops (WCNCW)*, Piscataway, NJ, USA: IEEE, 2020, pp. 1–6.
- [30] B. Teng et al., "Bayesian user localization and tracking for reconfigurable intelligent surface aided MIMO systems," *IEEE J. Sel. Topics Signal Process.*, vol. 16, no. 5, pp. 1040–1054, Aug. 2022.
- [31] A. Fascista et al., "RIS-aided joint localization and synchronization with a single-antenna receiver: Beamforming design and low-complexity estimation," *IEEE J. Sel. Topics Signal Process.*, vol. 16, no. 5, pp. 1141–1156, Aug. 2022.
- [32] Y. Han et al., "Large intelligent surface-assisted wireless communication exploiting statistical CSI," *IEEE Trans. Veh. Technol.*, vol. 68, no. 8, pp. 8238–8242, Aug. 2019.
- [33] C. Hu et al., "Two-timescale channel estimation for reconfigurable intelligent surface aided wireless communications," *IEEE Trans. Commun.*, vol. 69, no. 11, pp. 7736–7747, Nov. 2021.
- [34] K. Zhi et al., "Two-timescale design for reconfigurable intelligent surface-aided massive MIMO systems with imperfect CSI," *IEEE Trans. Inf. Theory*, vol. 69, no. 5, pp. 3001–3033, May 2023.
- [35] D. Dardari, M. Luise, and E. Falletti, *Satellite and Terrestrial Radio Positioning Techniques: A Signal Processing Perspective*. New York, NY, USA: Academic, 2011.
- [36] F. Guidi, A. Guerra, and D. Dardari, "Personal mobile radars with millimeter-wave massive arrays for indoor mapping," *IEEE Trans. Mobile Comput.*, vol. 15, no. 6, pp. 1471–1484, Jun. 2016.
- [37] C. Pan et al., "An overview of signal processing techniques for RIS/IRS-aided wireless systems," *IEEE J. Sel. Topics Signal Process.*, vol. 16, no. 5, pp. 883–917, Aug. 2022.
- [38] T. Hou et al., "Reconfigurable intelligent surface aided NOMA networks," *IEEE J. Sel. Areas Commun.*, vol. 38, no. 11, pp. 2575–2588, Nov. 2020.
- [39] G. Ghatak, "On the placement of intelligent surfaces for RSSI-based ranging in mm-wave networks," *IEEE Commun. Lett.*, vol. 25, no. 6, pp. 2043–2047, Jun. 2021.
- [40] D. Dardari et al., "Ranging with ultrawide bandwidth signals in multipath environments," *Proc. IEEE*, vol. 97, no. 2, pp. 404–426, Feb. 2009.
- [41] Z. Sahinoglu, S. Gezici, and I. Guvenc, *Ultra-Wideband Positioning Systems: Theoretical Limits, Ranging Algorithms, and Protocols*. New York, NY, USA: Cambridge University Press, Jan. 2008, pp. 1–269.
- [42] F. Saggese, M. Moretti, and A. Abrardo, "A quasi-optimal clustering algorithm for MIMO-NOMA downlink systems," *IEEE Wireless Commun. Lett.*, vol. 9, no. 2, pp. 152–156, Feb. 2020.
- [43] D. Dardari, P. Closas, and P. M. Djurić, "Indoor tracking: Theory, methods, and technologies," *IEEE Trans. Veh. Technol.*, vol. 64, no. 4, pp. 1263–1278, Apr. 2015.
- [44] Y. Bar-Shalom, X. R. Li, and T. Kirubarajan, *Estimation With Applications to Tracking and Navigation: Theory Algorithms and Software*. Hoboken, NJ, USA: Wiley, 2004.
- [45] A. Guerra et al., "Near-field tracking with large antenna arrays: Fundamental limits and practical algorithms," *IEEE Trans. Signal Process.*, vol. 69, pp. 5723–5738, 2021.
- [46] A. Guerra, F. Guidi, and D. Dardari, "Single-anchor localization and orientation performance limits using massive arrays: MIMO vs. beamforming," *IEEE Trans. Wireless Commun.*, vol. 17, no. 8, pp. 5241–5255, Aug. 2018.
- [47] T. Li, M. Bolic, and P. M. Djurić, "Resampling methods for particle filtering: Classification, implementation, and strategies," *IEEE Signal Process. Mag.*, vol. 32, no. 3, pp. 70–86, May 2015.
- [48] B. D. Anderson and J. B. Moore, *Optimal Filtering*. Mineola, NY, USA: Dover Publication Inc., 2005.
- [49] D. P. Bertsekas, *Nonlinear Programming*. Belmont, MA, USA: Athena Scientific, 1999.
- [50] S. Dwivedi et al., "Positioning in 5G networks," *IEEE Commun. Mag.*, vol. 59, no. 11, pp. 38–44, Nov. 2021.
- [51] "Study on NR positioning support," 3rd Generation Partnership Project (3GPP), Sophia Antipolis, France, Tech. Rep. 38.855, 10, version 16.0.0, 3GPP-R16, 2019.
- [52] K. N. Nguyen et al., "Beam management with orientation and RSRP using deep learning for beyond 5G systems," in *Proc. Int. Conf. Commun. Workshops (ICC Workshops)*, 2022, pp. 133–138.
- [53] Y. Gao et al., "Gyro-net: IMU gyroscopes random errors compensation method based on deep learning," *IEEE Robot. Autom. Lett.*, vol. 8, no. 3, pp. 1471–1478, Mar. 2023.
- [54] P. Tichavsky, C. H. Muravchik, and A. Nehorai, "Posterior Cramér-Rao bounds for discrete-time nonlinear filtering," *IEEE Trans. Signal Process.*, vol. 46, no. 5, pp. 1386–1396, May 1998.